D.2.2.1. REPORT ON METAL ADDITIVE MANUFACTURING RESULTS

DATE: 24/01/2023

www.additool.eu

Contenido

INTRODUCTION

The Work Package 2 (WP2) of the ADDITOOL project with Title: *Technology transfer from MAM to the tooling sector* proposed to develop and fabricate 5 pilots to transfer the AM technologies to SMEs of the tooling sector in the SUDOE. In the Activity 2.2: *Fabrication, post-processing and characterization of the demonstrators*, all the partners have worked together to develop 5 pilots.

In this report all the results, conclusions and recommendations obtained in the 5 pilots are explained.

OBJECTIVE

The main objective of this document is to compile the results obtained in this Industrial research phase of the ADDITOOL project following the information detailed in D.1.3.1. Set of case studies about each pilot.

DESCRIPTION

During this task, 5 pilots have been developed attending to the Terms of Reference defined in the Activity 1.3. Each pilot was leaded by different technological centres and uses different technologies and materials in order to cover different industry interests. A matching between centres and technologies was performed to develop interesting pilots for AM technology transfer. The results are summarised in the following stages: manufacturing, post processing and characterisation.

In the Table 1, the selected technologies, participants, and leader of each pilot are detailed.

Table 1. Pilot, use case proposing company, leader and participants of each pilot.

Participants	FR1 LAUAK	PT1 MOLDETIPO	SP1 MEUPE/INESPASA	FR2 SOMOCAP	PT2 VIDRIMOLDE
ESTIA	LEADER				
CEIT					
LORTEK				LEADER	
UPV/EHU					
CATEC			LEADER		
IPLEIRA		LEADER			LEADER
CEFAMOL					
ENIT					

RESULTS

Pilot FR1-LAUAK

DED WIRE LASER

Before manufacturing the part, it was important to develop all the set of parameters for manufacturing the 15CDV6 with DED Wire Laser technology considering at least:

- Laser Power
- Wire speed
- Travel speed

But also:

- Massic density energy (DME)
- Surface density energy (DSE)
- Energy per unit length (DLE)

SUIVI D'ESSAI - PRECITEC							
Date	04/05/22	Opérateur(s)	VP	PS	PD		
Heure	11:40						
Machine	COMAU	Matériau	15CDV6				
Numéro fiche	22XXX	Densité (g/cm3)	8,12				
Numéro d'affaire/projet	ADDITOOL	Diamètre fil (mm)	1,2				
Numéro substrat	/	Dimension substrat (mm)	150x150x5				
Référence matière	/	Dimension pièce (mm)	/				

Préparation du substrat	Sablage	Inertage (PPM O2)	Début essais /		Résultats
			Fin essais /		
Objectif	Recherche de paramètres procédé pour le 15CDV6	Distance focale (couronne/substrat)	105 mm		
Opération de vérification	Centrage laser/fil	Oui	Répartition de puissance	Oui	Redresseur	Non

Référence	Type (cordon, mur, bloc, pièce)	Puissance laser W	Vitesse robot mm/min	Vitesse robot m/s	Vitesse fil m/min	Vitesse fil kg/h	Delta_z mm	Delta_xy mm	Temporisation s	Observations et commentaires	Validation (OK, NOK)
ADDITOOL_C1	Cordon de 50mm	3000	1500	0,025	1,50	0,83	/	/	/	pression argon : 0,3 bar et distance retract : 3mm	OK
ADDITOOL_C2	Cordon de 50mm	3000	1500	0,025	2	1,10	/	/	/	pression argon : 0,3 bar et distance retract : 4mm DEFAUT: pas de retract et fil sorti du redresseur santé CORDON : largeur variable	NOK
ADDITOOL_C3	Cordon de 50mm	3000	1500	0,025	2,00	1,10	/	/	/	pression argon : 0,3 bar et distance 4mm. Rajout d'une tempo 0,2s entre wireStop et laserStop	OK
ADDITOOL_C4	Cordon de 50mm	3000	1250	0,021	2,00	1,10	/	/	/	pression argon : 0,3 bar + distance 4 mm + tempo 0,2s DEFAUT : variation largeur cordon	OK
ADDITOOL_C5	Cordon de 50mm	3000	1250	0,021	2,50	1,38	/	/	/	pression argon : 0,3 bar + distance 4 mm + tempo 0,2s DEFAUT : boule. Fil trop bas au départ.	NOK
ADDITOOL_C6	Cordon de 50mm	3000	1250	0,021	2,50	1,38	/	/	/	pression argon : 0,3 bar + distance 4 mm + tempo 0,2s DEFAUT : trop d'apport de fil	NOK
ADDITOOL_C7	Cordon de 50mm	3500	1250	0,021	2,50	1,38	/	/	/	argon : 0,3 + dist 4mm + C4 avec augmentation puissance laser +16,6% légère boule sur la fin et légères irrégularités dans le cordon	OK
ADDITOOL_C8	Cordon de 50mm	3750	1250	0,021	2,50	1,38	/	/	/	argon : 0,3 + dist 4mm + C4 avec augmentation puissance laser +25%	OK
ADDITOOL_C9	Cordon de 50mm	4000	1250	0,021	2,50	1,38	/	/	/	argon : 0,3 + dist 4mm + C4 avec augmentation puissance laser +33,3%	OK
ADDITOOL_C10	Cordon de 50mm	4000	1500	0,025	2,50	1,38	/	/	/	argon : 0,3 + dist 4mm + retour à vitesse robot 1500 mm/s	OK
ADDITOOL_C11	Cordon de 50mm	5000	1500	0,025	2,50	1,38	/	/	/	argon : 0,3 + dist 4mm + retour à vitesse robot 1500 mm/s + 1000W de puissance en +	OK
ADDITOOL_C12	Cordon de 50mm	5500	1500	0,025	2,50	1,38	/	/	/	argon : 0,3 + dist 4mm + retour à vitesse robot 1500 mm/s + 1500W de puissance en +	OK
ADDITOOL_C13	Cordon de 50mm	5500	1500	0,025	4,00	2,20	/	/	/	argon : 0,3 + dist 4mm DEFAUT : apport de fil trop important, pliage du fil en amont des galets redresseurs	NOK
ADDITOOL_MF1	Mur fin	3000	1500	0,025	2,00	1,10	0,50	/	/	parametrie C3 DEFAUT : fil bloqué dans le dévidoir	NOK
ADDITOOL_MF2	Mur fin	3000	1500	0,025	2,00	1,10	0,50	/	/	paramétrie C3 mur très insatisfaisant sans raison valable	NOK
ADDITOOL_C14	Cordon de 50mm	3000	1500	0,025	2,00	1,10	/	/	/	argon : 0,3 + dist 4mm parametrie C3 pas de tir. Laser non prêt	NOK
ADDITOOL_C15	Cordon de 50mm	3000	1500	0,025	2,00	1,10	/	/	/	argon : 0,3 + dist 4mm parametrie C3 pas de tir. Laser non prêt	NOK
ADDITOOL_C16	Cordon de 50mm	3000	1500	0,025	2,00	1,10	/	/	/	argon : 0,3 + dist 4mm parametrie C3 parfait	OK
ADDITOOL_MF3	Mur fin	3000	1500	0,025	2,00	1,10	0,50	/	/	parametrie C3 DEFAUT : boule sur fil à mi-cordon à la 3 eme couche	NOK
ADDITOOL_MF4	Mur fin	3000	1500	0,025	2,00	1,10	0,50	/	/	parametrie C3 DEFAUT : boule sur fil à la 2eme couche	NOK
ADDITOOL_MF5	Mur fin	2500	1500	0,025	2,00	1,10	0,50	/	/	diminution de la puissance laser DEFAUT : goutte fil à cause du redresseur	NOK
ADDITOOL_MF6	Mur fin	2750	1500	0,025	2,00	1,10	0,50	/	/	augmentation puissance laser DEFAUT : goutte	NOK

Ilustración 1 : Research of parameters

This first step will allow to find the best weld bead to manufacture at the end the part and 4 walls for characterization with the following dimensions:

- 115 x 15 x 95mm
- 80 x 20 x 100mm
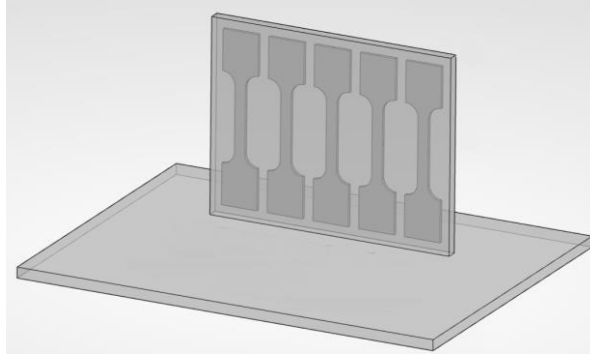- 100 x 20 x 90mm

- 85 x 25 x 50mm

Ilustración 2 : Wall for characterization

The characterization will give us data according to:

- Microstructure gradient from top to bottom
- Hardness
- Tensile properties in the vertical orientation
- Tensile properties in the horizontal orientation
- Etc.

All the results of microstructure and mechanical tests are available on the report D.2.1.1.: Report on material for MAM.

In terms of search of parameters, the 15CDV6 material can have a lot of problems with oxidation and generate a lot of spatters even with a laser deposition. A modification of the PRECITEC head have been done for the local shielding to protect the weld bead.
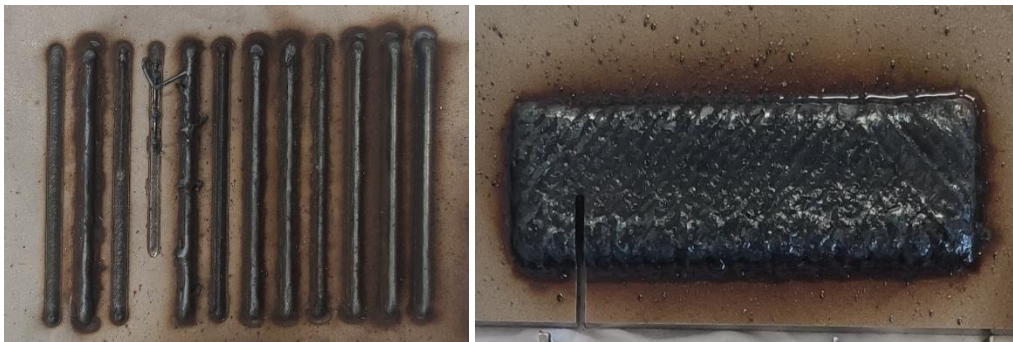
Ilustración 3 : Example of oxydation

The effect of the shielding (local and global) has a consequent effect on the deposition and on the parameters. The better the shielding is, the more the material reflects the laser, and the power must be increased.

However, with a too high Laser power, sublimation can happen creating smoke which can contaminate the effector. However, it is important to find the process limits and find the best "shooting window".
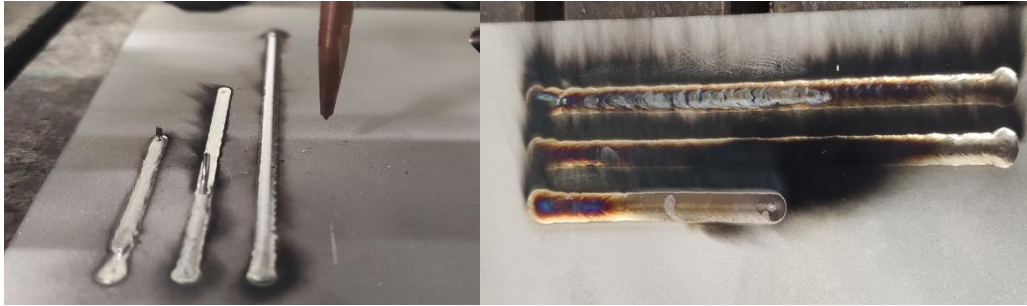
Ilustración 4 : Sublimation of the material

In terms of deposition, the strategy also influences the geometrical aspect as well as the microstructure.

For this deposition, to avoid having porosities or surface defects, some strategies have been developed:

- 0° longitudinal go and back
- +45°/-45° with contouring
- +45°/-45°without contouring
- -135°/+120°/-45°/+60°/45°/-60°/135°/-120° without contouring to avoid surface defects

Ilustración 5 : Influence of the deposition strategy

The contouring can be a problem to obtain a homogenous surface on the top and respect the stick out on all the part. A big difference between the contour and the filling creates a loss of the stick out and the process stops.

Ilustración 6 : Example without contourning

Once all the parameters were set, a little redesign was done to create a Near Net Shape and include the final part inside.
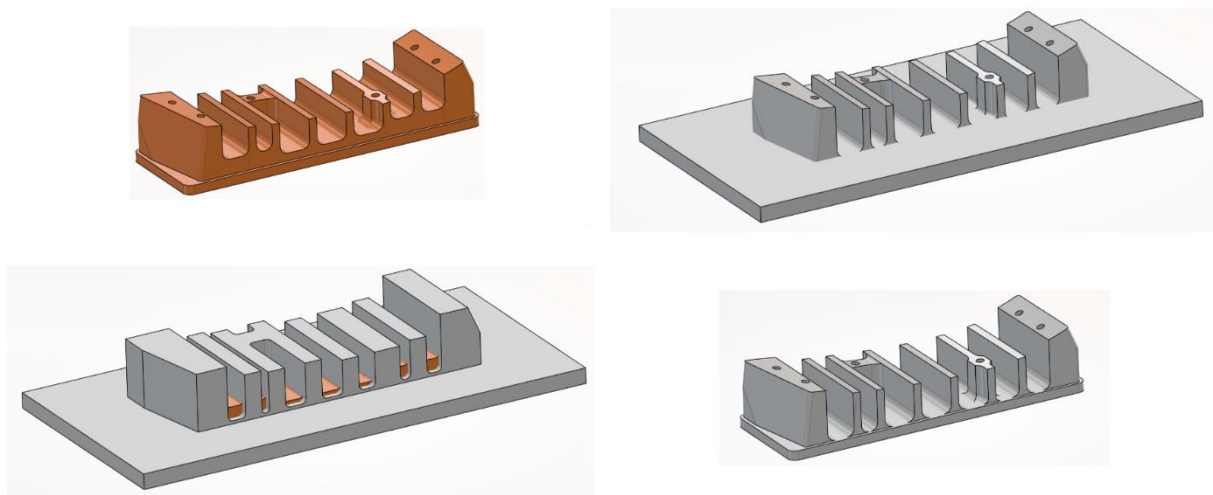
Ilustración 7 : Near Net Shape

The manufacturing of this part has been done with:

- Robot COMAU NJ165
- PRECITEC CoaxPrinter
- Wire SelectArc 15CDV6 – Diameter 1.2mm.

Ilustración 8 : Manufacturing of the NNS with DED Wire Laser

Once the manufacturing was done, a 3D Scan was performed to see the different deviation between CAD and reality. The 3D Scan has been done before and after the Thermal Treatment.

The TT performed was a stress relieving during 8 at 400 °C.

- Maximum deviation between CAD and NNS: 1.8mm
- Maximum deviation between NNS before and after TT: 0.204mm
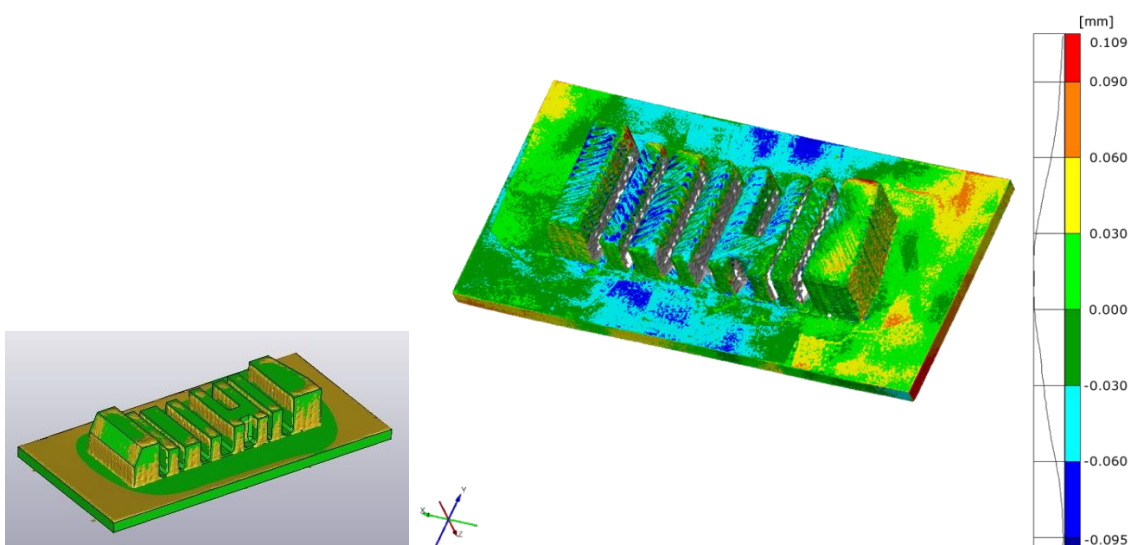
Ilustración 9 : Scan 3D

The deviation before and after TT, even if it is small (0.2 mm) proves that a relaxation of the stresses has indeed taken place in the part and that the machining will be carried out without risk of cracking.
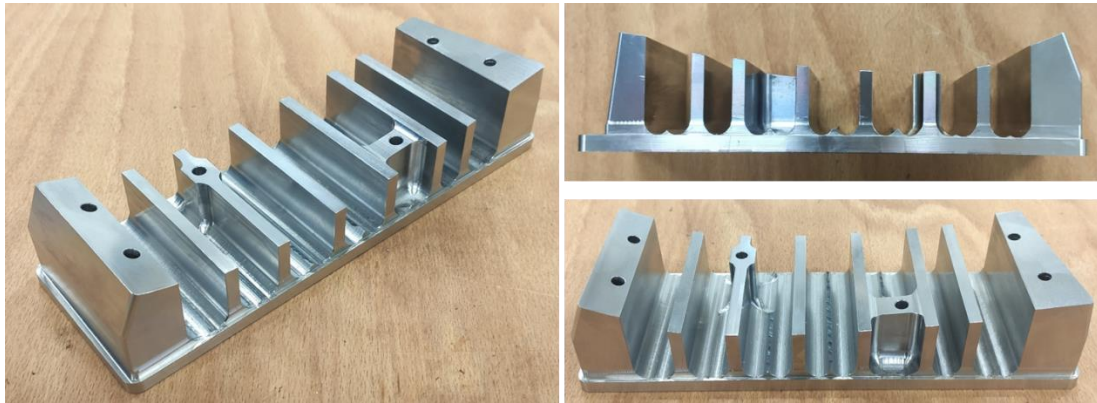
Ilustración 10 : Machining of the DED WL part

Finally, the part being finished, the last phase was the control and the functional tests on this tooling.

A few points remain outside the initial tolerances due to non-compliance with the dimensions (machining provided by subcontracting) but largely acceptable by the LAUAK company, the definition of the tolerances being voluntarily very tight.
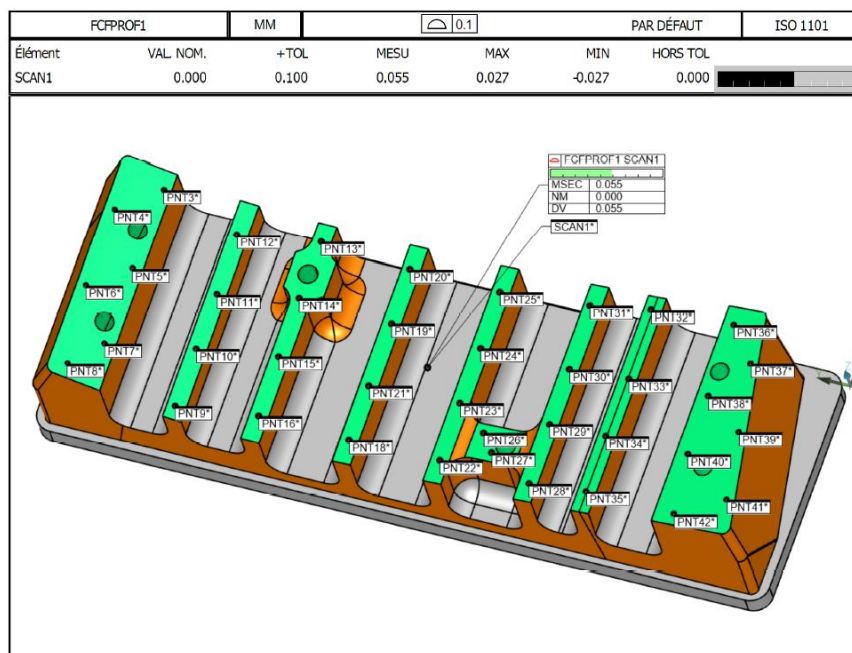
Ilustración 11 : Contrôle et tests par LAUAK

The part is now functional and used by the LAUAK company.

DED WIRE ARC

The manufacturing process was done by:

- Fanuc Robotic arm
- CMT Fronius welding equipment
- Wire SelectArc 15CDV6 – Diameter 1.2mm.

The following method was applied to develop the strategies for the part manufacturing by DED Wire Arc:

➢ Optimisation of the parameters with 15CDV6 material. Soundness and geometry of the weld beads was checked.

Figure 1. Unitary weld beads and cross section.

The selected parameters for the manufacturing of the walls are shown in the next Table:

Table 2. Selected parameters for the manufacturing of walls.

W speed (cm/min)	WFS (m/min)	Current (A)	Voltage (V)
40	6,2	200	15,5

Two different robot movement were used in order to select the one that obtain the thickness required (>6 mm): two overlapped weld beads and circling. Surface machining was done to see how removing the least possible material, the required wall thickness was obtained.
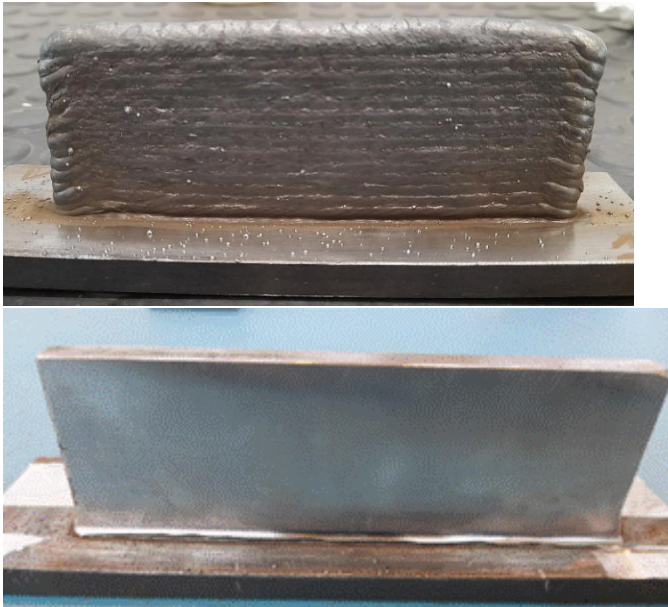
Figure 2. NNS walls manufactured before and after machining of the surfaces.

➢ After the characterisation of the microstructure and mechanical properties, circling strategy was selected as it achieved a homogenous microstructure in the whole wall.

A big wall was done to analyse the mechanical properties in two orientations.

Figure 3. Manufactured wall.

➢ Redesign of the part with over thicknesses (1 mm on each side of walls) considering the material that has to be removed by machining.

The main purpose followed was to reduce as much as possible the deposited material, hence the walls were descended to the substrate and two stringers were added to prevent distortions in each edge of the part.

Original design   Optimised design
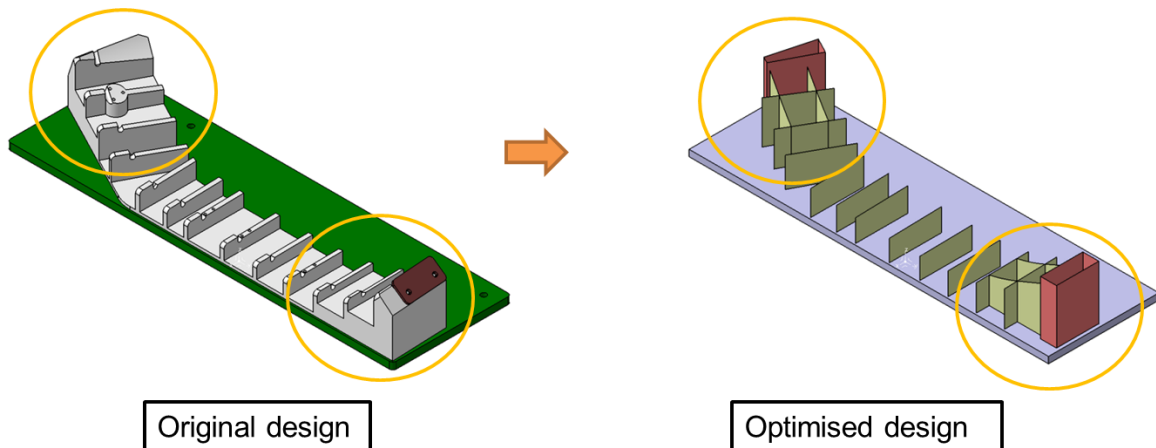
Figure 4. Original design and optimised redesign for WAAM.

Details were manufactured to optimise the intersection between walls.

Figure 5. Detail manufacturing for the optimisation of the strategy.

➢ Programming the robot path with oscillations to reduce the distortions. The sequence of the manufacturing is planned to homogenise the heat in the part.
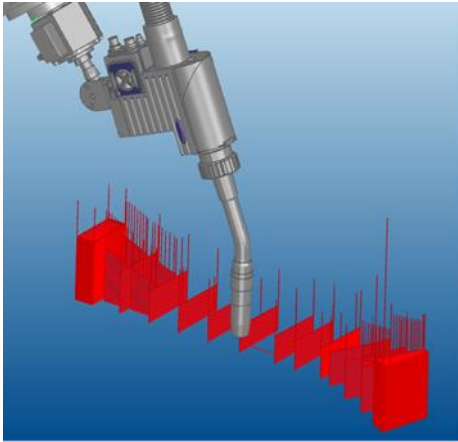
Figure 6. *Simulation of the robot path planning for part manufacturing.*

➢ Run thermal and distortion simulations to define the interlayer dwell time and robot path planning that optimised the manufacturing strategy to reduce the distortions during the manufacturing step.

The selected interlayer dwell time was variable along the part growth in order to avoid heat accumulation. As we go upper in height the dwell time had to be increased to assure a limit temperature of the part bellow 150 °C.
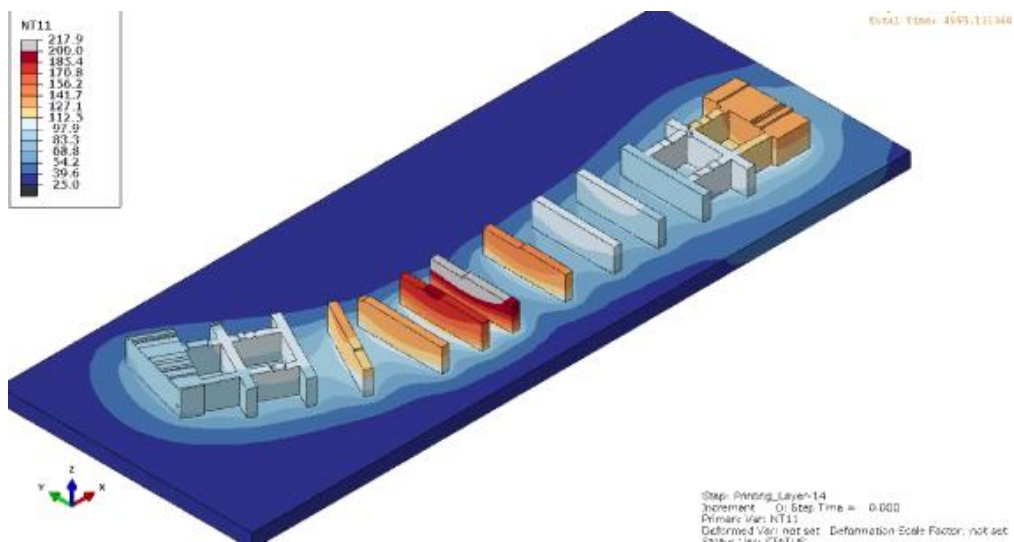

Figure 7. Temperature simulation after de deposition of each layer.

The expected deformation showed how the part should be machined to meet with the dimensional requirements.
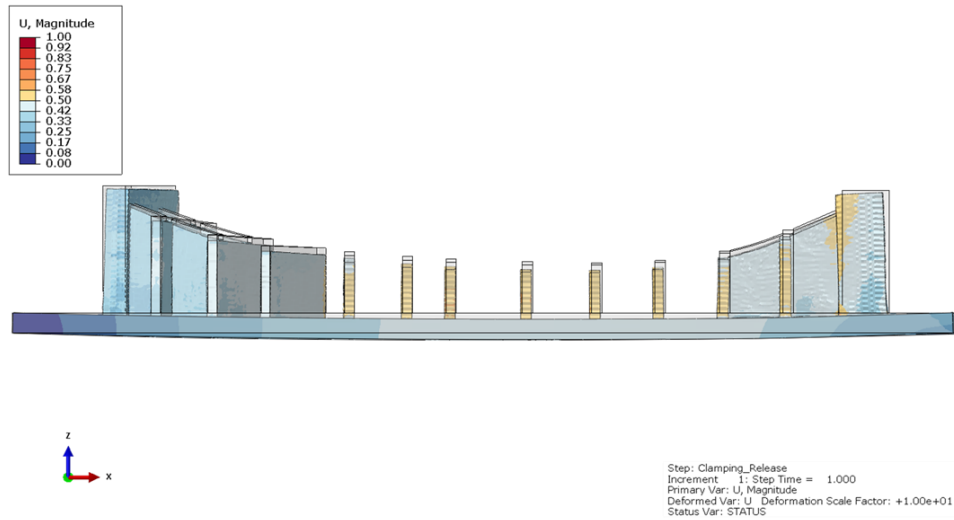
Figure 8. *Distortion simulation after removing from clamps.*

➢ Design of the clamping tooling. L shape clamp with bolts were used on each side of the substrate.
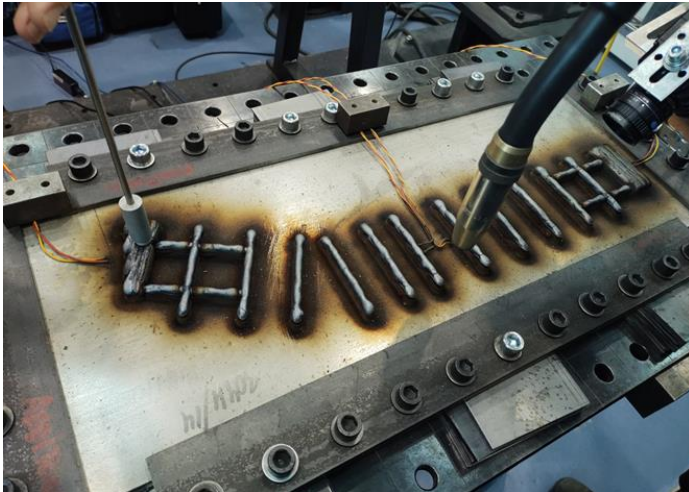

Figure 109. *Fabrication of the demonstrator and monitoring of the temperature.*

➢ Manufacturing of the part was done with CMT technology and robotic arm on a substrate of 650 x 250 x 14 mm of 304.
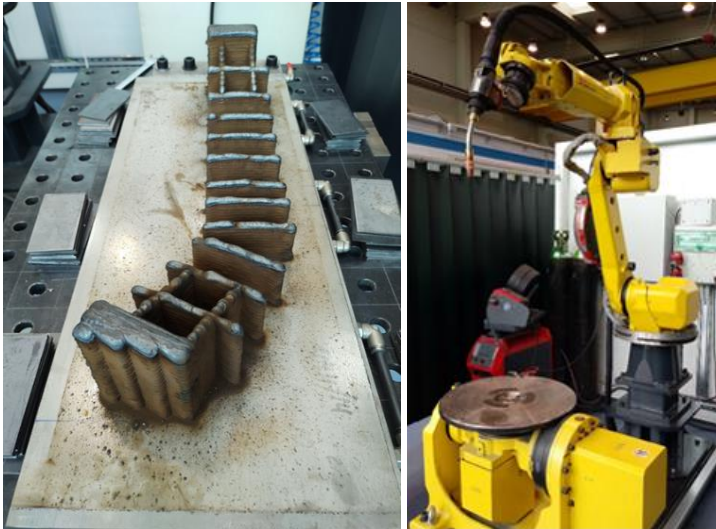
Figure 10. Manufactured part and the robot used for its manufacturing.

➢ Monitoring of the temperature and melt pool.

4 K-type thermocouples were attached to the substrate and a contact thermocouple were used to monitor the temperature at the top on the walls between each layer deposition and compare the values with the simulation results.
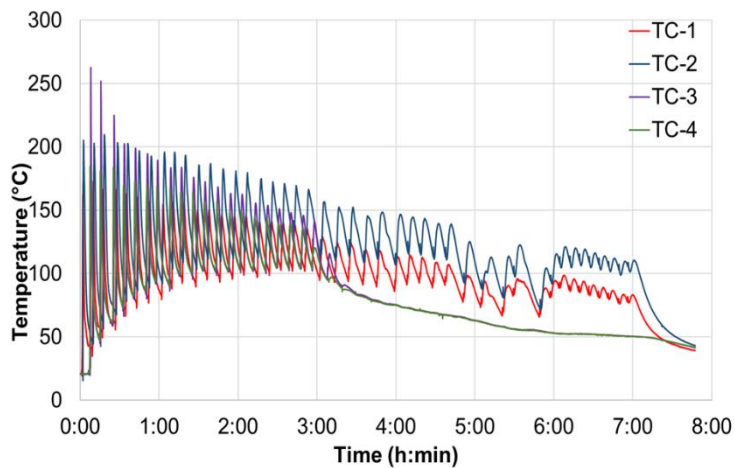

Figure 11. Temperature record chart obtained from K-type thermocouples of the substrate.

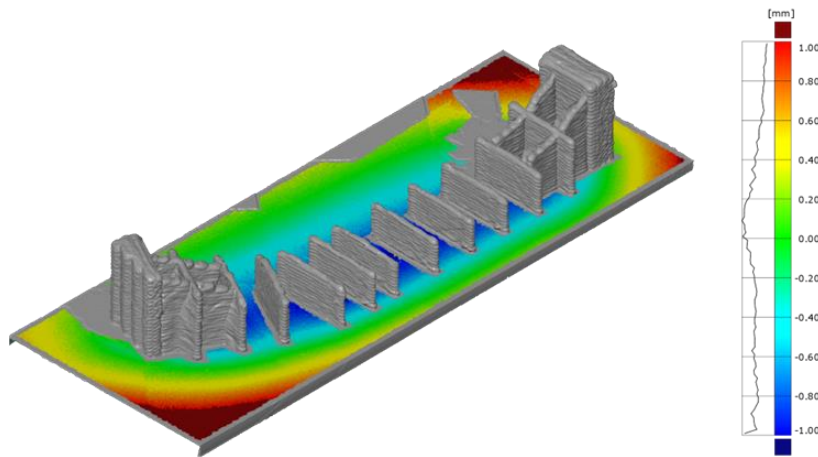➢ Dimensional analysis and best fit after the manufacturing.

Figure 12. Best fit of the distortion suffered by the substrate.

➢ Machining of the part. During the machining new distortions appeared due to the residual stresses.

Figure 13*. Machined critical zones of the demonstrator.*

➢ Dimensional analysis after the machining and best fit of the critical surfaces has been done.
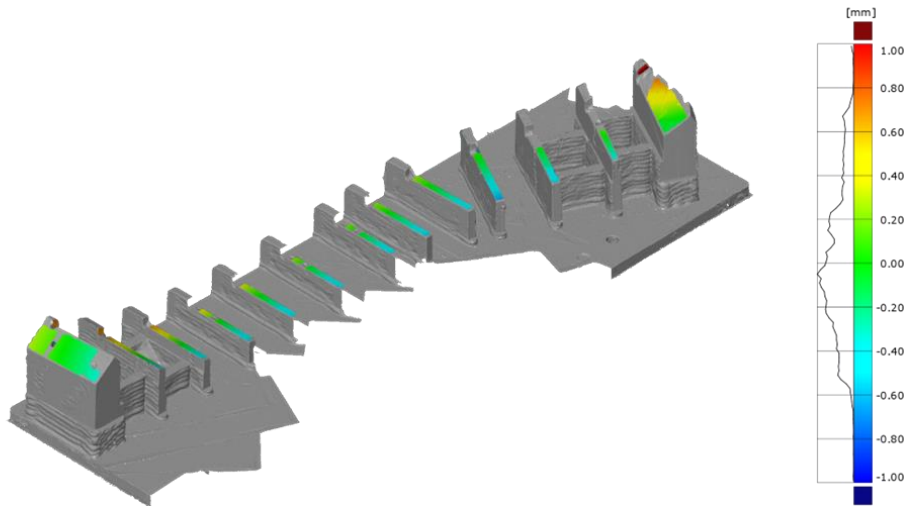
Figure 14. Best fit of the critical zones machined.

A few points remain outside the scheduled tolerances but expected to be acceptable by the LAUAK company, because the definition of the tolerances was very tight.
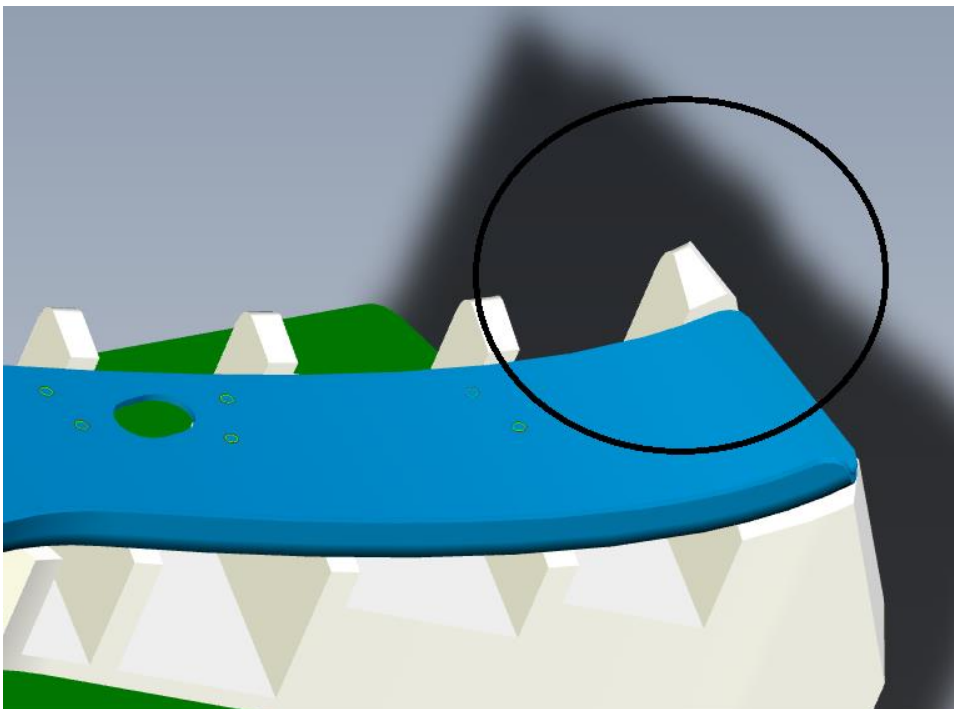

Figure 15. Zone out of tolerances.

DED POWDER LASER

The atomised powder was characterized in the technological centre CEIT, ensuring a morphologically adequate, low porosity, low satellite powder, with a particle size between 44-106 µm and mean diameter of 73 µm.

The following methodology was applied:

> **Optimisation of the parameters with 15CDV6 material. Single clad and overlapped clad tests.**

The optimal values for the laser power (P), travel speed (F) and powder feed rate (Q) are established through the single clad tests. For the Design Of Experiments (Table 5), a 3 factor 3 level methodology is used, employing the deposition parameters for H13 as central values:

Table 5: Single clad test DOE for 154CDV6 deposition by L-DED.

	P (W)	F (mm/min)	Q (g/min)
Ref.	600	450	3.3
Max	700	550	4
Min	500	350	2.6

From the 27 single clads the optimal clad is chosen based on:

- Metallurgical integrity
- Adequate geometry (H/W value near 0.25)
- A dilution value near 30%

Based on the previous criteria, the optimal values of the deposition parameters are determined to be: P = 600 W, F = 550 mm/min and Q = 3,3 g/min. The clad fabricated by this parameter set is shown in Figure 13. The height of the clad is of 0.229 mm, the width 1,234 mm and the dilution depth of 0.184mm.
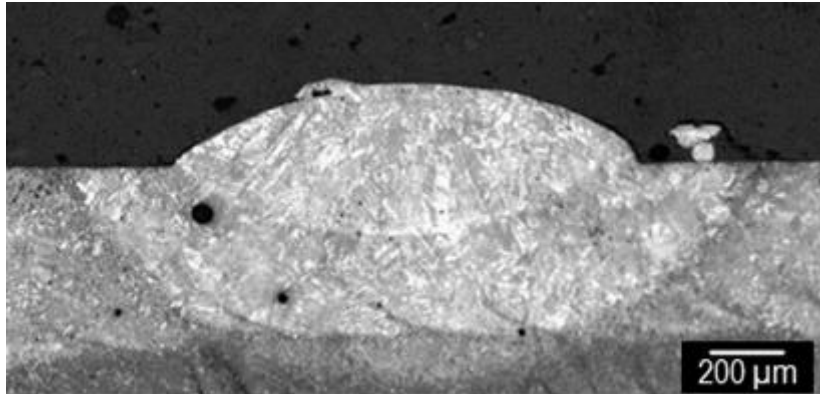
Figure 13: cross section of the single clad fabricated with optimal parameters.

Four layers are fabricated employing the parameters above and each setting an overlap of 30%, 35%, 40% and 45% between successive clads. The optimal overlap value must compromise a regular layer height with maintaining sufficient dilution on the substrate, which for the 15CDV6 material is 40%. Figure 14 shows the cross section of the optimal overlap layer.
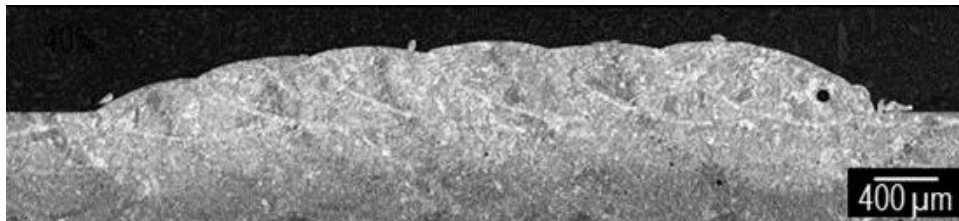

Figure 14: optimal layer fabricated with an 40% overlap.

> **Deposition strategy testing through wall fabrication**.

In order to test the best deposition strategy, three 6x30x15 walls are fabricated with the strategies shown in Figure 15. The first layer is fabricated without optimised cooling breaks while the other them every 8 layers.
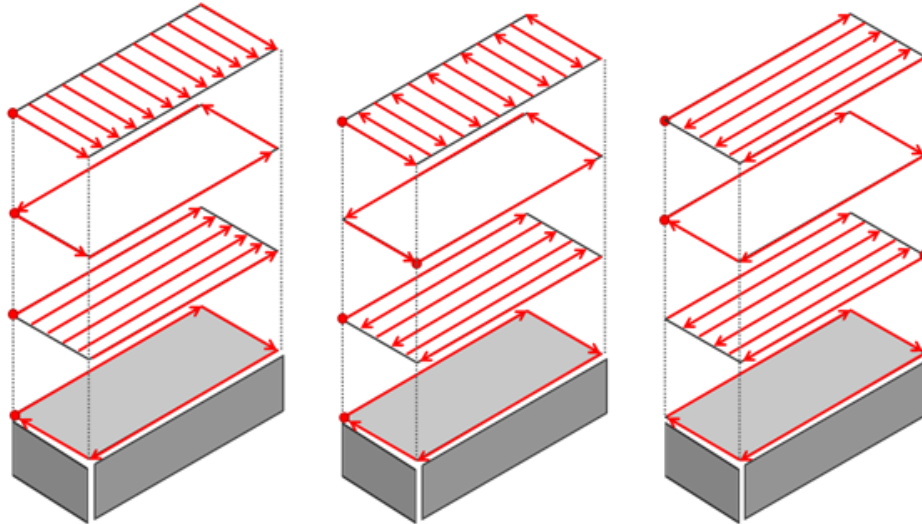
Figure 15: Deposition strategies testes during wall fabrication

The second wall in, which material was deposited in the longitudinal and transversal directions in ZigZag for the infill, showed the most uniform height and the best geometrical accuracy, given the uniformity of the thermal field created in the fabrication process. The three cross sections are shown in Figure 16 .
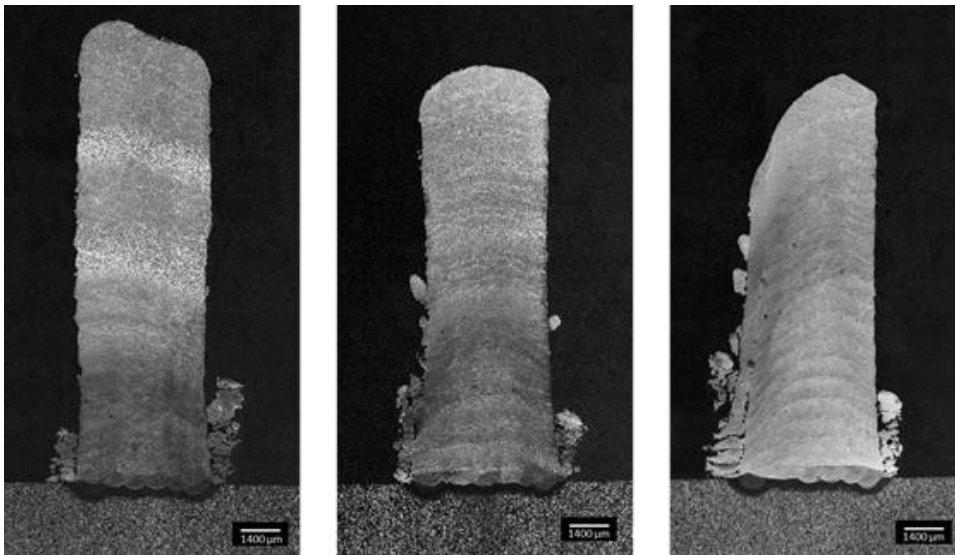

Figure 16: cross sections of the fabricated walls.

➢ **Microstructure and microhardness characterisation.**

A microstructural analysis of the deposited material has revealed the creation of Acicular Ferrite during the process. The formation of this microstructure is encouraged by the fast thermal cycles of L-DED and the alloying elements present in the 15CDV6 material.

The relationship between cooling times and the presence of Acicular Ferrite is observed in Figure 17, where is shown that the material deposited while the substrate is overheated has a coarser grain with more ferrite content. After cooling breaks, the material dissipates heat efficiently again and the previous microstructure is achieved.

The formation of Acicular Ferrite is also related to elevated mechanical properties in the deposited material, with an average microhardness value of 40 HRC.
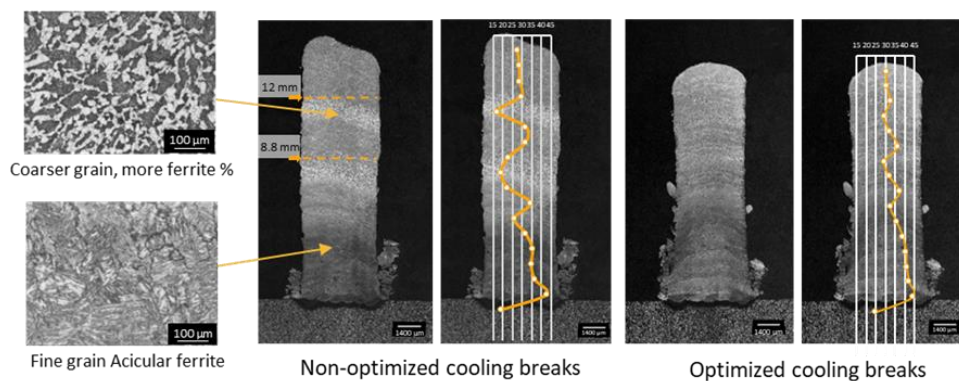

Figure 17: microstructure, cooling times and micro hardness values for the walls fabricated with and without cooling breaks.

➢ **Demonstrator part fabrication.**

The demonstrator part is fabricated from a machined preform of AISI1045 material. The process was carried out using reference parameters previous developed which give 0.4mm clad height with 40% overlapping strategy. The active faces have been machined an additional 2 millimeters to prepare for the 15CDV6 coating and final machining.

During the fabrication process the part is tilted to enable for the nozzle to reach the deposition surface, as shown in Figure 18.

Figure 18: Demonstrator part fabrication setup in L-DED.

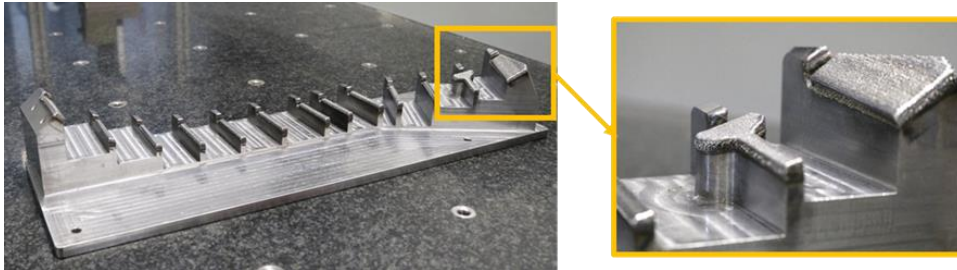Figure 19 shows the demonstrator part before the post processing step.

Figure 19: Demonstrator part after 15CDV6 coating in L-DED.

The coated part is partially machined, in order to demonstrate different stages of the fabrication process. The post-processed faces have a dimensional accuracy of 0.1mm and a Ra between 1.5 and 2. The hardness measured in the post processed faces is of 42 HRC.

The learnt lessons in the development of this demonstrative pilot are:

Defect free and sound parts were manufactured using MAM technologies applying different strategies:

- **Hybridization** of machining and MAM. This has the advantage of reducing the difficulty of machining in specific zones and having the possibility to use highly added value materials just in the required zones and a cheaper material in the rest.
- **Redesign** for MAM. This has the advantage of reducing the mass of the part by around 30 %.

Redesign is essential to obtain the advantages from MAM:

- material savings
- low waste of material
- short lead time

Simulation enhances the deposition strategies to reduce distortions. In these terms, temperature and residual stress simulations were run to assure proper manufacturing without distortions or collapse. However, it is very important also to know the final distortion of the part to optimise the overthickness to meet the dimensional requirements after the machining step.

Pilot PT1-MOLDETIPO

Manufacturing

The mold insert of Pilot PT1 was manufactured by L-PBF in a Trumpf TruPrint 1000 equipment. The part was manufactured using Böhler W360 powder, a tool steel whose properties are equivalent to H13 steel.

Before the manufacturing of the part itself, specimens from the same material were produced, to perform mechanical, microstructural and thermal characterisation. The results from this task can be consulted in the deliverable D 2.1. REPORT ON MATERIAL FOR MAM.

For both the manufacturing of the part and of the specimens, the processing parameters are described in Table XXX. The part obtained is depicted in figure ZZ.

Table XXX: L-PBF processing parameters used in the manufacturing of the insert.

Area / Zones	Parameters: travel speed and LASER power
Core (inside of the part)	700mm/s | 120W
Downskin (non-supported areas)	460mm/s | 30W
Inskin Hatch (overlap between the outer layer and the inside of the part)	700mm/ | 120W
Inskin Border (outer layer)	500mm/s | 80W

Post-processing

The post processing of the part involved the separation from the base plate, via wire EDM. This was performed at a local company (EROFIO) who possesses the appropriate equipment for this task. No heat treatment was performed.

After this, the part was sent to Moldetipo, where milling, EDM and detail adjustment operations prepared the part for assembly in the mould. These operations were like the ones the conventionally manufactured insert went through. Figure FFF depicts the final state of the insert.

Figure FFF: Final geometry of the L-PBF insert, after finishing.

After the manufacturing the insert was analysed by CT scan, to verify the interior geometry of the cooling channels and to check for any defects. A general view of the insert is shown in Figure DDD. It is possible to verify that the cooling channel was correctly obtained, and only minor surface roughness in the inside of the channel is detected.
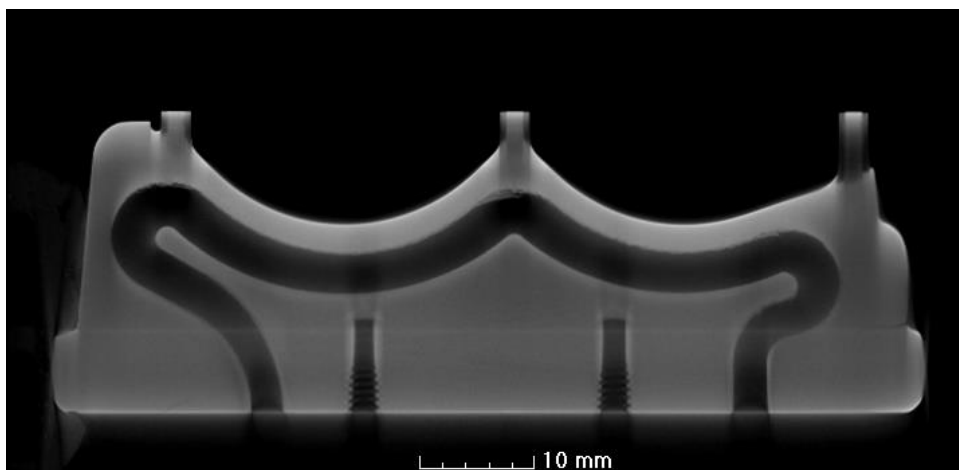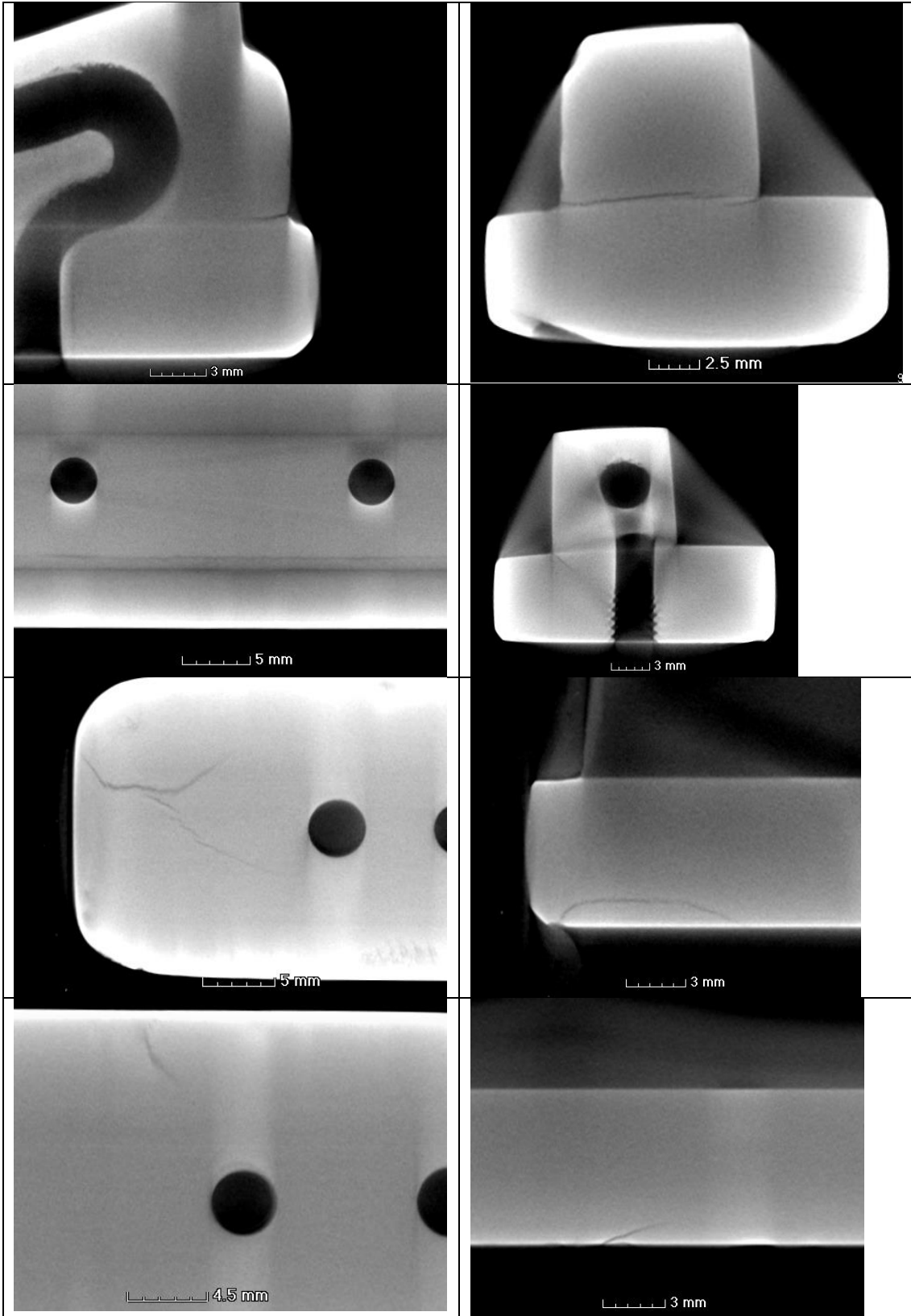

Figure DDd: Image of the L-PBF insert obtained by CT scan showing the internal cooling channel.

However, detailed analyses of the area that connects the base to the active surface of the insert reveal a series of cracks – figures DDD, RRR, TTT. Some of these cracks were visible at naked eye.

Characterisation of the demonstrator

Overall, the manufacturing of the demonstrator was successful. Moldetipo considered that the mould insert would lead to productivity gains for this part. Other parts could also benefit from this strategy. The cooling geometry was proven to affect the moulding cycle significantly and be economically viable – see results of D3.2.1 – Viability Study.

The learnt lessons in the development of this demonstrative pilot are:

The manufacturing of this pilot showed that it is possible use MAM technologies to obtain a functional part, for an industrial application, with higher performance than originally. The functionality was demonstrated despite the fact that some defects occurred. Thermal treatments should be considered for this kind of parts, to control the material structure and obtain higher toughness.

Pilot SP1-MEUPE/INESPASA

The redesign of the AM case of SP1 pilot (Figure 1) has been carried out considering:

- Internal channels with force air to decrease surface temperature of the case.
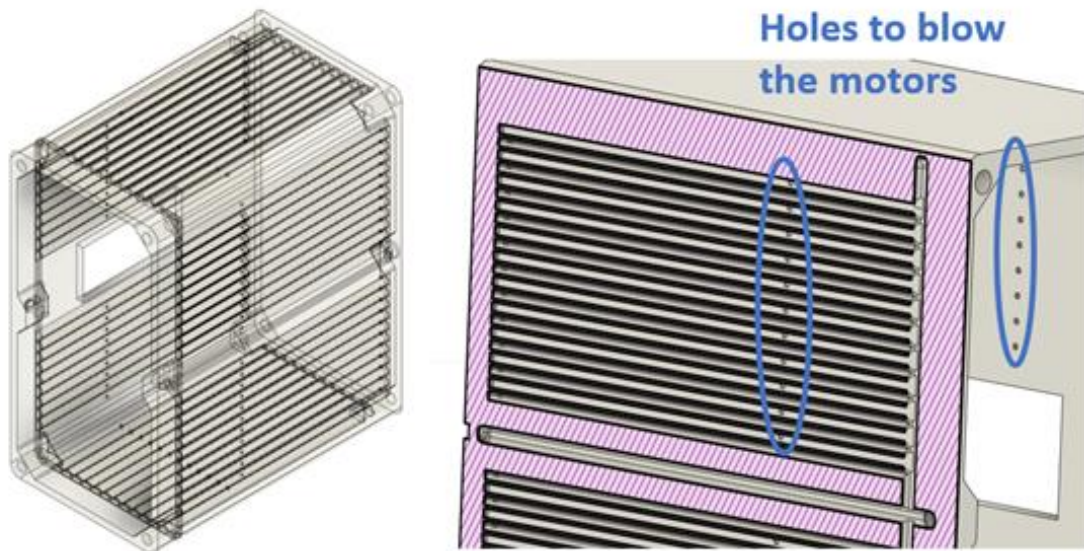- Holes to refrigerate the motors with air during operation.

Figure 1. Image of internal channels and motors refrigeration holes in SP1 design

Before the manufacturing of the AM case, several considerations have been taken into account:

- Results obtained in terms of Materials characterization presented in D 2.1 Report on materials for MAM
- Thermal results at coupon level also shown in D 2.1 Report on materials for MAM
- Thermal Simulation results on the case

Regarding the last, some thermal simulations have been performed in order to evaluate the behaviour of the whole drilling machine. On the contrary to the analysis performed at coupon level, in this case the conditions of the model are maintained constant, and the experimental test is only performed to determine the error of the model. Figure 2 shows the cross section of the AM manufactured casing. As it can be seen, after 50 minutes working, the temperature on the motor reaches almost 70°C, but thanks to the design of the external casing and the implemented forced convection system, the outer temperature remains below 25°C.
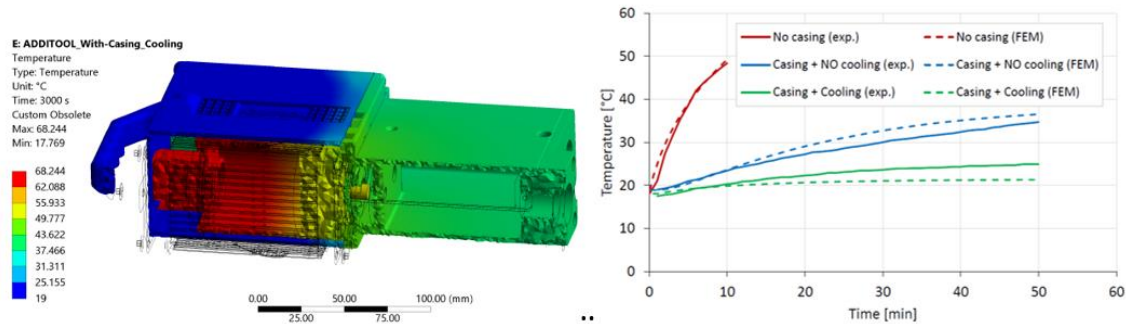
Figure 2. Cross-section of the thermal field of the drilling machine with the AM casing and the cooling activated (left). Comparison between the experimental and FEM temperatures (right).

The Pilots SP1 have been produce by Laser Powder Bed Fusion (LPBF) in a Renishaw platform (RenAM 500E). 2 different build jobs (BJ1 & BJ2) have been manufactured in Scalmalloy® with a layer thickness of 30 μm. The cases has been designed and orientated in the build plate to avoid support structure in order to minimize the manufacturing and post-processing time. Below, it can be observed the manufacturing (Figure 3-left) and extraction processes (Figure 3-right) of BJ2.
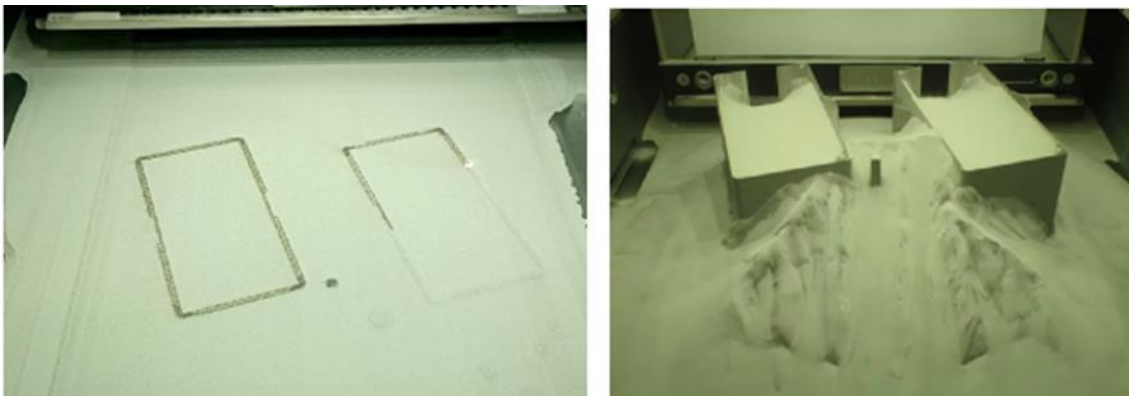

Figure 3. (Left) Manufacturing and (right) extraction processes of BJ2.

 3 cases have been manufactured in 2 different batches. BJ1 (Figure 4-left) has took 30h with a material consumption of 246g to produce demonstrator nr. 1 (D1), while BJ2 (Figure 4-right) has took 42h with a material consumption of 432g to manufacture demonstrators 2 and 3 (D2 and D3). The extraction of the occluded powder in the

internal channels in D1 and D3 has been performed through the holes designed to blow the motors.
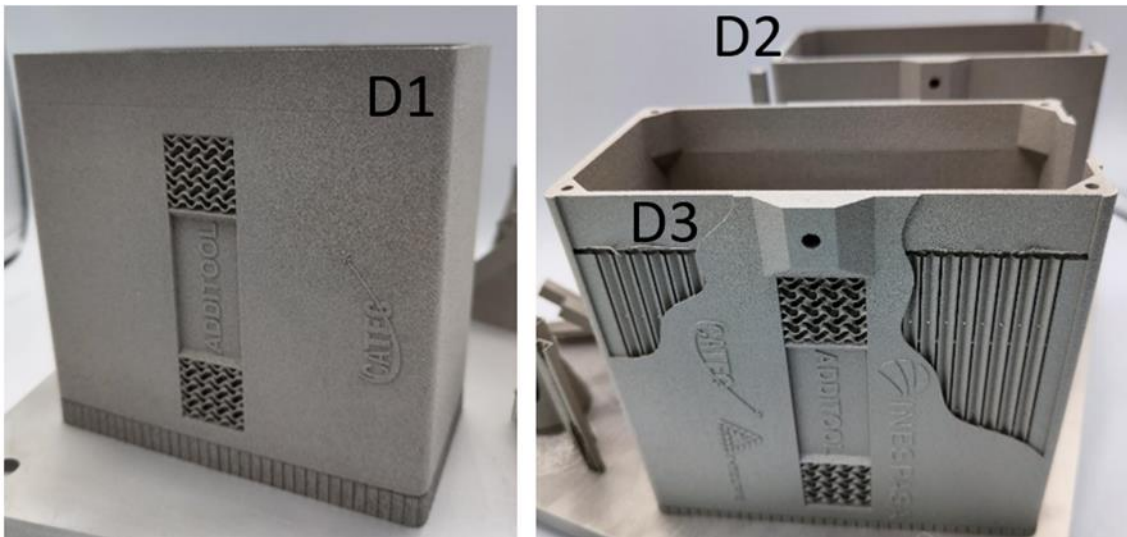

Figure 4. Image of (left) D1, (right) D2 and D3 still joined to the manufacturing plate.

D3 has been manufactured as a demonstrator to show the internal channels while D1 and D2 have been produced to demonstrate the solution with force air during operation.

In order to compare different process to obtain the interfaces (areas with higher dimensional requirements, highlight in red in Figure 5), 2 different post-processes have been considered:

- D1 interfaces and treads have been obtained by machining, (MEUPE facilities, Figure 6-left).
- D2 and D3 interfaces have been achieved by EDM-Electro Discharge Machining (Figure 6-right), and threads with a vertical drilling system (Figure 7).
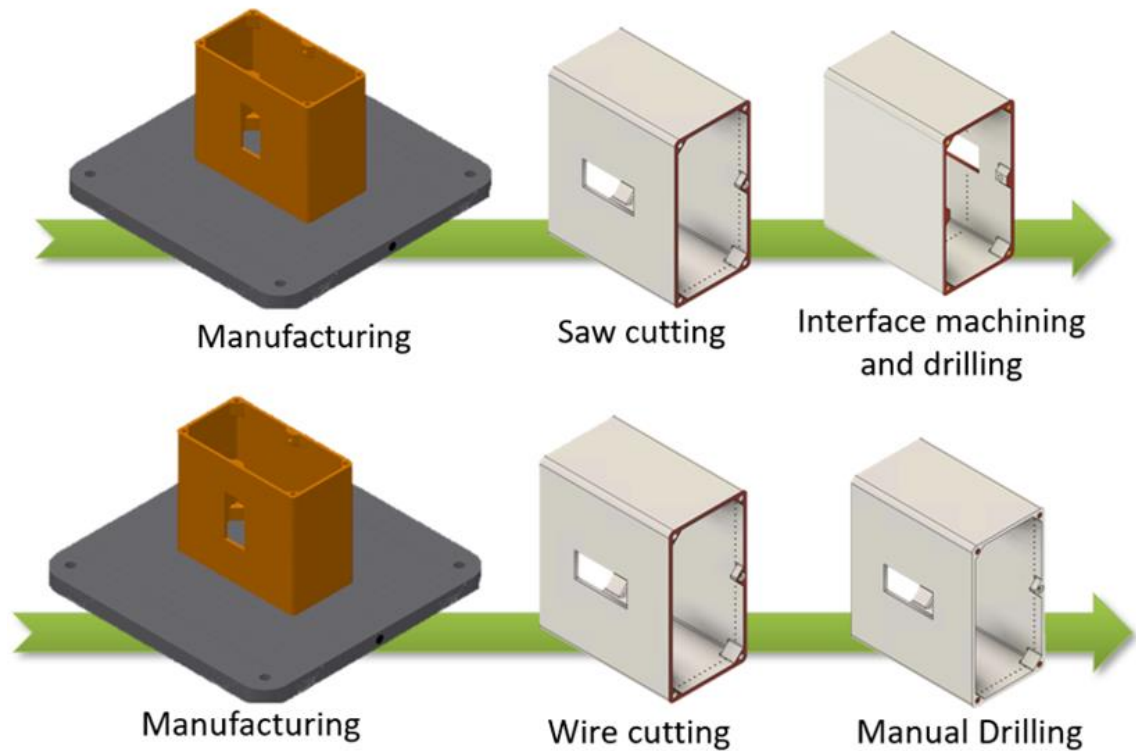
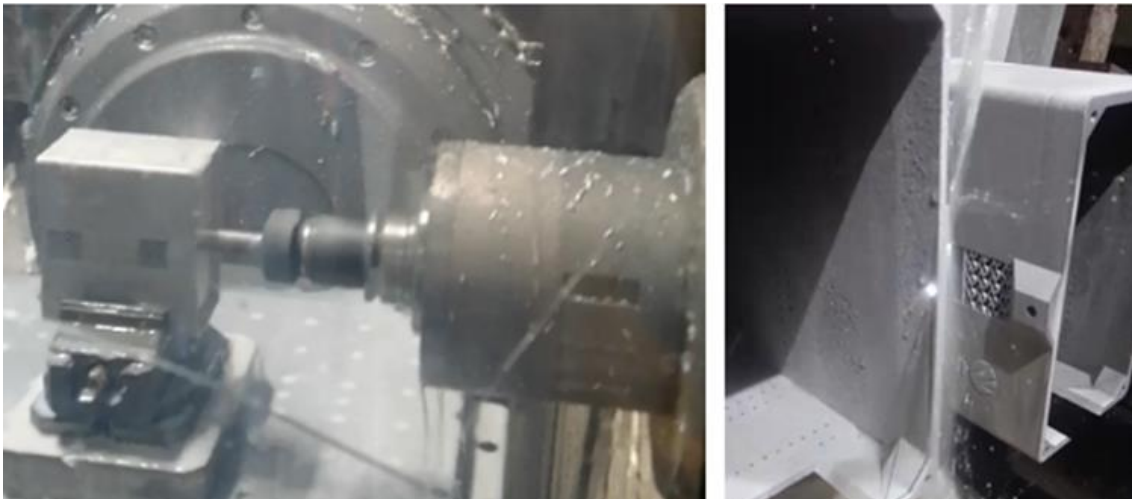*Figure 5. Post processing route of (up) D1, (down) D2 and D3.*

Figure 6.(left) Machining process of D1 interfaces and (right) interface achievement by EDM in D2 and D3
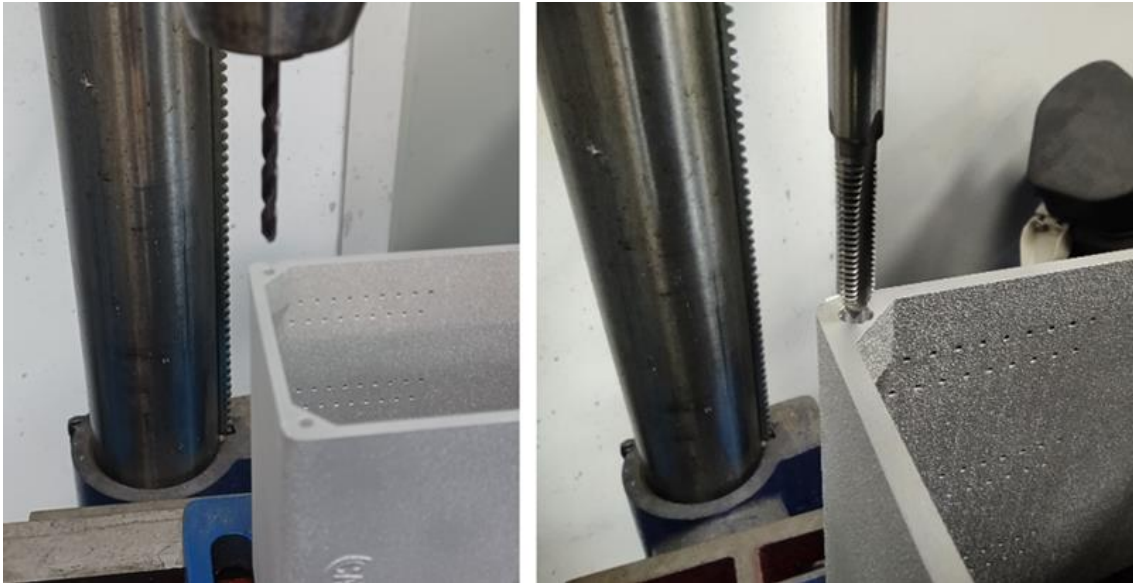
Figure 7.(left) Drills and (right) threads obtained manually for D2 and D3.

To assure that no powder is still occluded inside de internal channels, a chemical fluid has been induced trough the inner cavities. A nitric - hydrofluoric acid have been used only for 5 minutes to avoid thickness reduction and maintaining structural integrity. Below, it can be observed the demonstrators after the cleaning process (Figure 8).
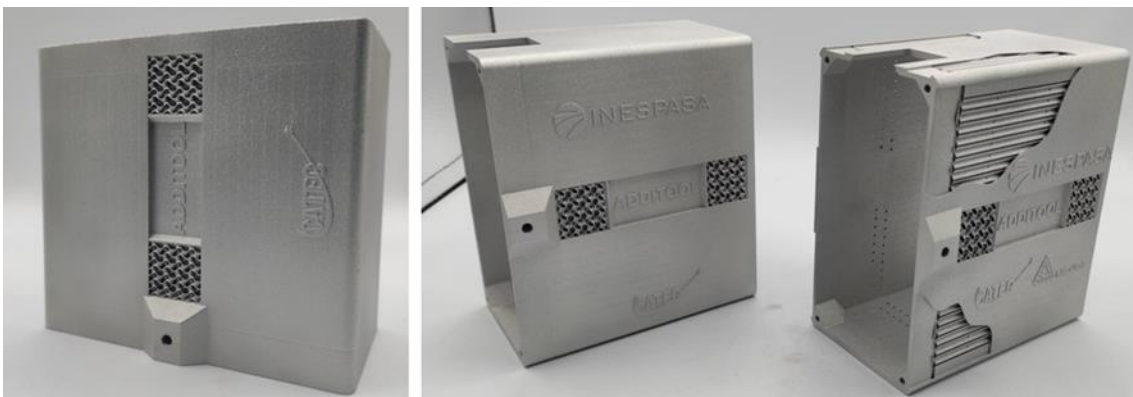
Figure 8.Images of (left) D1, (right) D2 and D3 after the cleaning process

All of them were inspected by computed tomography, which is the only nondestructive technique capable to show dimensional deviations in internal cavities, and also to assure that no powder was occluded inside the components. Figure 9 present 2D cross section and 3D representation of the results acquired by computed tomography performed in D1. To obtained the 3D deviation analysis, a comparison analysis between the nominal CAD (orange in Figure 9) and the 3D CT data set (grey in Figure 9) have been performed.

It is stated that no occluded powder remains inside the channels, and no significant deviations are observed.
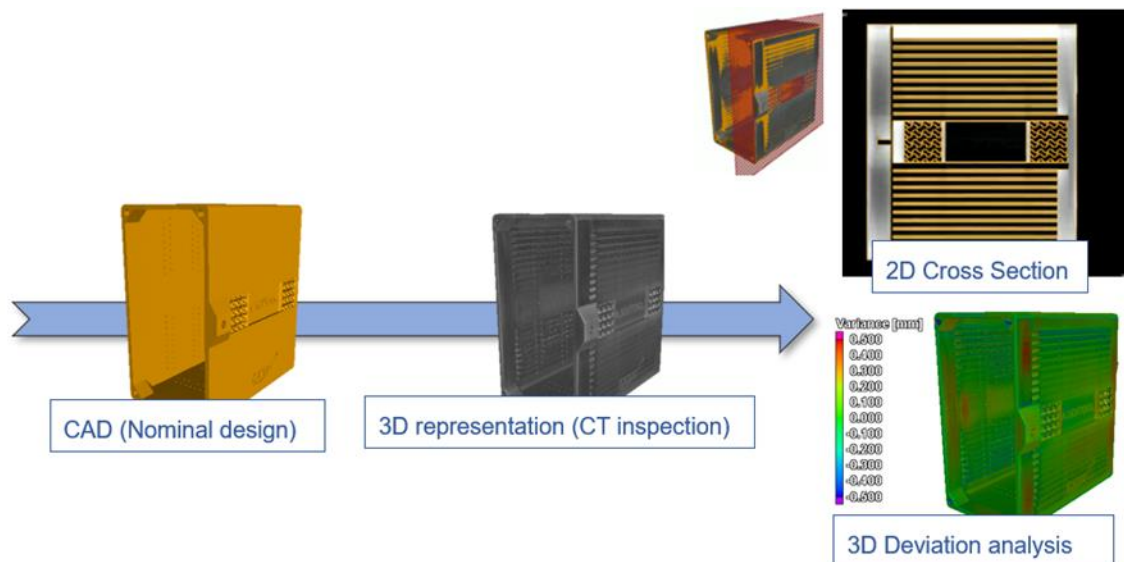
Figure 9.CT inspection results of D1

Several experimental tests have been performed to validate the AM solution. An infrared thermography camera and a thermocouple have been used to monitor the thermal behavior during operation. Both cases, conventional and redesign with internal channels, have been analyzed working during 50 minutes with the motors operating at 300 rpm. Figure 10-left top (indication B) shows the conventional case reaching 55°C in 50 minutes while the maximum temperature achieved in the AM case with force air after 50 minutes working is 25°C (Indication A, Figure 10-left bottom).

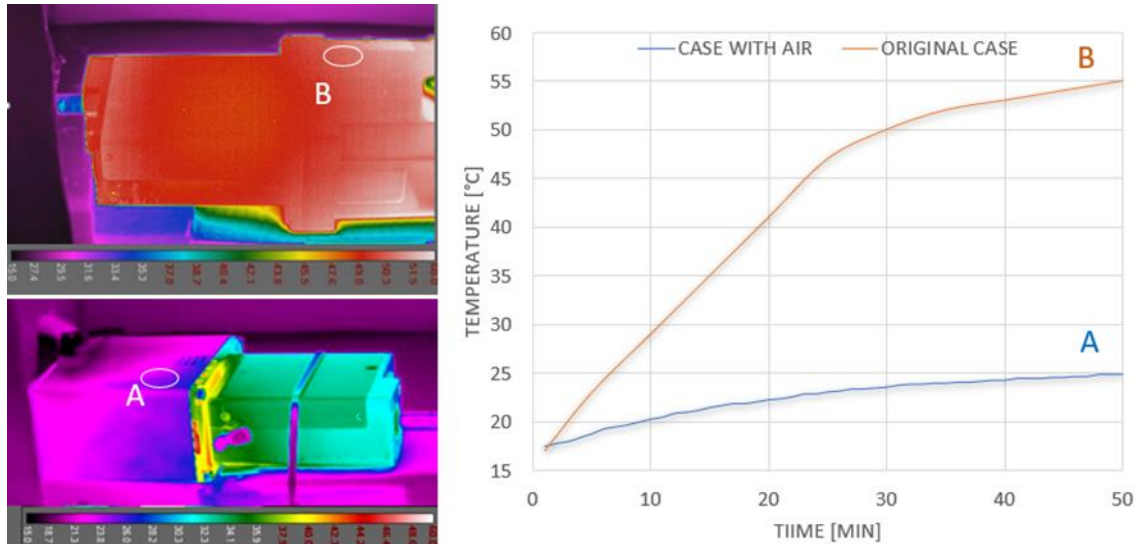*Figure 10.Thermographic images of (left top) conventional and (left bottom) AM redesigned cases. (right) Comparative graph of thermocouples.*

Additional tests have been performed to analyze the behavior of the AM case while operating without force air. In this case, it reaches 40°C after 50 minutes working (Indication C, Figure 11) instead of 55°C registered in the conventional case. At this point, if air is induced inside the channels, the case reaches 25°C in less than 10 minutes (Indication D, Figure 11).
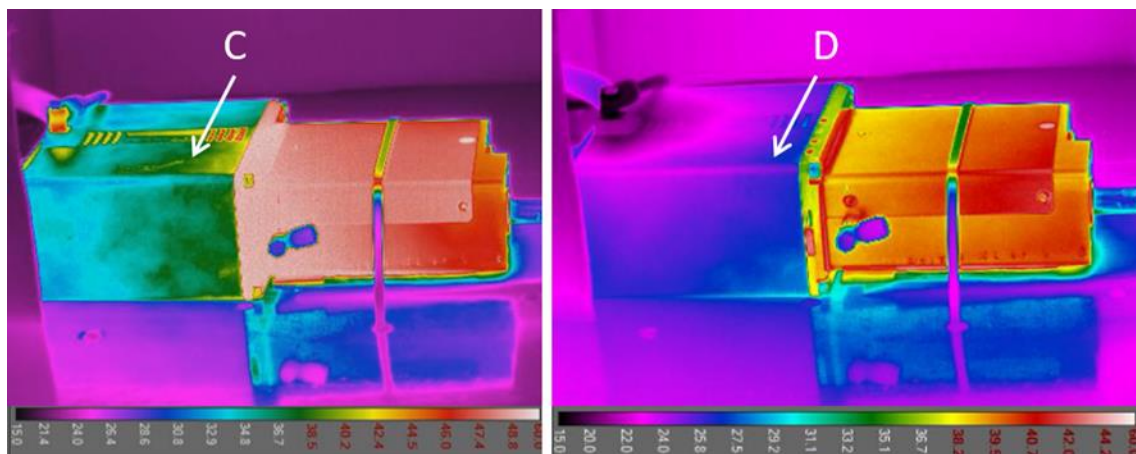

Figure 11.Thermographic images of AM case (left) operating without force air and (right) during cooling down process inducing air.

If we compare thermal simulations with the test performed on the conventional and AM case, it can be seen in Figure 12 overall good agreement between the model and the experimental data.
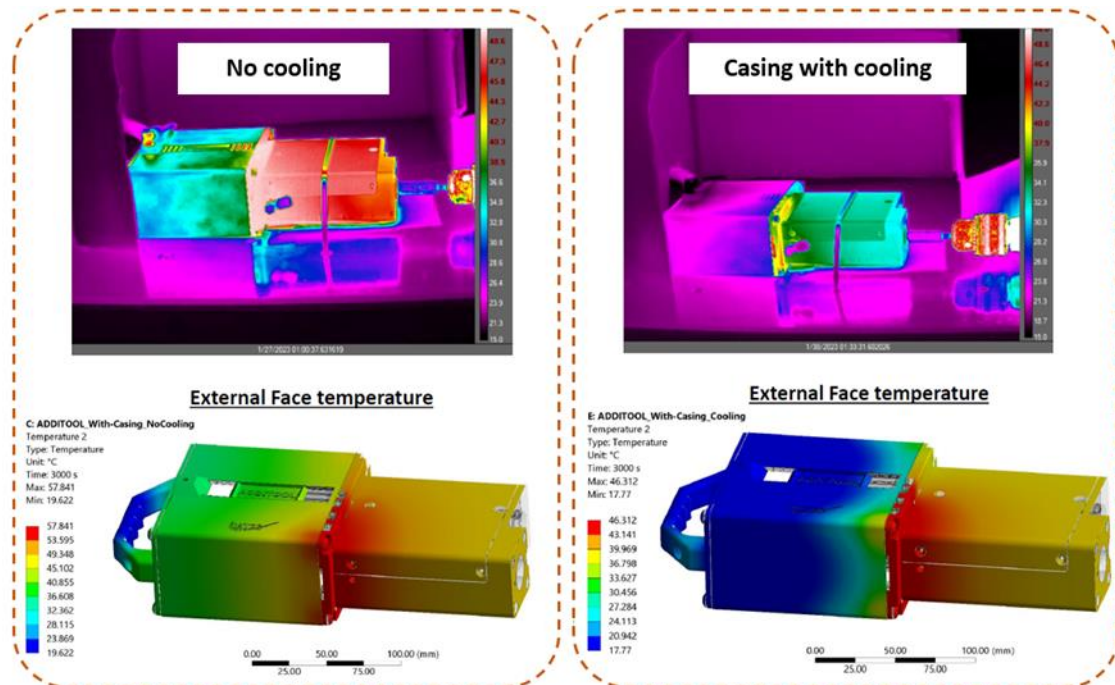
Figure 12. Comparison between experimental and simulation behaviour.

Regarding lessons learned during the development of this pilot, final tests have shown the improvement of thermal behavior in terms of heat dissipation by introducing internal cooling. In terms of warming up during operation, differences of 15°C by comparing Conventional case with new design and 30°C if introducing force air. If AM case is used without forced air, in less than 10 min it could be operative again (after 50 minutes working).

Regarding weigh of the component, by using AM case with internal channels a reduction of 37% has been achieved.

Moreover, thermal simulations have demonstrated a close match between experimental and simulated results in the AM case. This approximation could be very interesting in case a new design is proposed, for instance, by redesigning the entire case, not only where the motors are located. In this context, the thermal performance of the case could be checked before manufacturing, avoiding additional experimental tests to validate the component.

Pilot FR2-SOMOCAP

The technology being new for an open system, it was necessary to start from the beginning and make some adaptations:

- Development with the machine Lynxter S600D + NANOE H13 filament (abort development of the NANOVIA 316L because not enough mechanical properties).
- Several tests of printing + debinding + sintering with a cubic oven (Argon +2.5% Hydrogen atmosphere).
- Printing of samples for CEIT to improve debinding and sintering.
- Redesign of the part taking into account all the design rules (Discussion loop with SOMOCAP with the modification of the cooling channel diameter and correlation with the simulation).
- Negotiation with other new companies to develop a new H13 or 17-4PH paste (see Deliverable 2.3.1 Viability study).

1) Modification of the S600D + NANOE H13

The machine being originally mounted in "Bowden", it was necessary to make modifications to the hardware to transform it into a "Direct Drive". Indeed, given the fragility of the filament (loaded at more than 50% in volume in metallic powder), a "Direct Drive" machine is recommended, with a nozzle of 0.8mm in steel to prevent it from becoming clogged.

This modification allowed to find all printing parameters before purchasing the new extrusion tool (developed by Lynxter) – see **¡Error! No se encuentra el origen de la referencia.**.
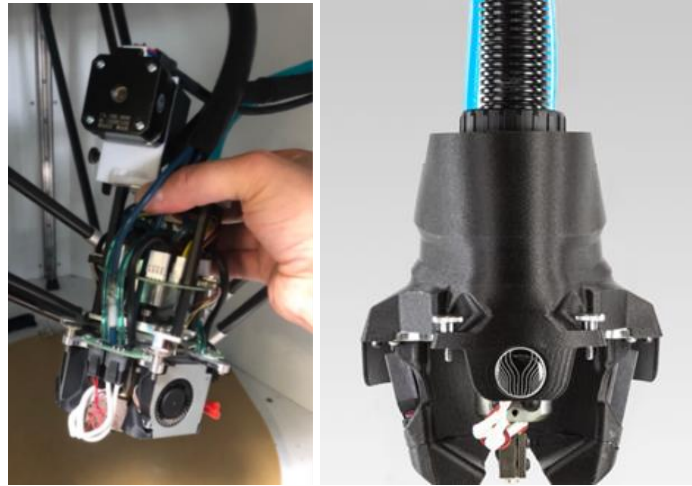
Figure 16 : Modification of the triple extrusion in Direct Drive

Thanks to the parameter's identification, see **¡Error! No se encuentra el origen de la referencia.**, the parametry for the printing is the following:

- Nozzle diameter: 0.8mm
- Extrusion multiplier: 115%
- Extrusion width: 0.8mm
- Layer height: 0.2mm
- Infill: 100%
- Outline overlap: 50%
- Temperature of the nozzle: 183°C
- Temperature of the bed: 35°C
- Temperature of the chamber: 25°C
- Cooling: 10%
- Speed: 15mm/sec

| Test N°	Extruder			Layer					Infill					Temperature		Cooling	Speed	Commentaires	
	Nozzle Dia	extrusion multiplier/ co	extrusion width/ mm	layer/mm	Top Solid	bottom Soli	Outline: Perimete	Internal Fill	External Fill	Interior Fill	Outline Overlap	Infill Extrusion	T°c buse	T°c plateau	Layer/%	mm/s		
1	0,8	1,14	0,8	0,2	5	5	5	Rectilinear	Concentric	0	45	100	180	30	0	20	couche arrachée/grinding sur filament	
2	0,8	1,3	0,8	0,2	5	5	5	Rectilinear	Concentric	0	45	100	180	30	0	20	couche arrachée/grinding sur filament	Plaquette 30x30x3mm
3	0,8	1,3	0,8	0,2	5	5	5	Rectilinear	Concentric	0	45	100	180	30	0	20	couche arrachée/grinding sur filament	
4	0,8	1,3	0,96	0,2	5	5	5	Rectilinear	Concentric	0	45	100	180	30	0	20	couche arrachée/grinding sur filament	
5	0,8	1	0,8	0,2	5	5	5	Rectilinear	Concentric	0	45	100	180	30	0	15	couche arrachée/grinding sur filament	
6	0,8	1	0,8	0,2	5	5	5	Rectilinear	Concentric	0	45	100	180	30	0	15	Pas d'adhérence sur plateau	
7	0,8	1	0,8	0,2	5	5	5	Rectilinear	Concentric	0	45	100	180	35	0	15	dimensionnel ok avec optimization point	
8	0,8	1	0,8	0,2	5	5	5	Rectilinear	Concentric	0	45	100	180	35	0	15	dimensionnel ok avec Random point	
9	0,8	1	0,8	0,2	5	5	5	Rectilinear	Concentric	50	45	100	180	35	0	15	Défaut cohésion couche	
10	0,8	1	0,8	0,2	5	5	5	Rectilinear	Concentric	0	45	100	180	35	0	15	Défaut cohésion couche	
11	0,8	1,07	0,8	0,2	5	5	5	Rectilinear	Concentric	0	45	100	180	35	0	15	Défaut cohésion couche	Modelle dia 20 ep 3mm
12	0,8	1,1	0,8	0,2	5	5	5	Rectilinear	Concentric	0	45	100	180	35	0	15	Défaut cohésion couche	
13	0,8	1,12	0,8	0,2	5	5	5	Rectilinear	Concentric	100	45	100	180	35	0	15	cohésion couche Perfectible	
14	0,8	1,14	0,8	0,2	5	5	5	Rectilinear	Concentric	0	45	100	180	35	0	15	cohésion couche Perfectible entre perimetre et remplissage grinding sur filament	
15	0,8	1,14	0,8	0,2	5	5	5	Rectilinear	Concentric	0	50	104	180	35	0	15	grinding sur filament	
16	0,8	1,14	0,8	0,2	5	5	5	Rectilinear	Concentric	0	50	100	180	35	0	15	Bonne cohésion couche Perimère	
17	0,8	1,16	0,8	0,2	5	5	5	Rectilinear	Concentric	0	50	100	180	35	0	15	Pas bonne cohésion centre Solid et grinding sur filament Nettoyage Buse et Heat-break	
18	0,8	1,16	0,8	0,2	5	5	5	Rectilinear	Concentric	0	50	100	183	35	0	15	Bonne cohésion de couche	
19	0,8	1,15	0,8	0,2	5	5	5	Rectilinear	Concentric	0	50	100	183	35	2/20%	15	Périmètre délaminé	
20	0,8	1,15	0,8	0,2	5	5	5	Rectilinear	Concentric	0	50	100	183	35	2/10%	15	Bonne cohésion de couche	

Figure 17: Parameters identification

2) Tests of printing + debinding + sintering

Several samples have been printed including:

- Cubes.
- Walls (to see the maximum thicknesses able to be debinded and sintered).
- Cylinders.
- Cube with hole inside.
- Lattice structure.
- Traction samples.
- Cylinders with cooling channels – Loop with the redesign phase to see the quality of the deposition.
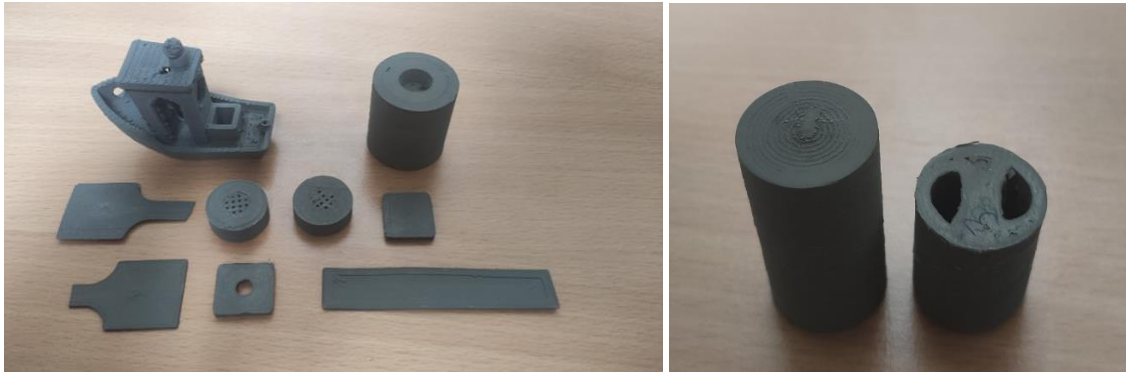- "Benchy boat" to validate the good printing.
- Etc.
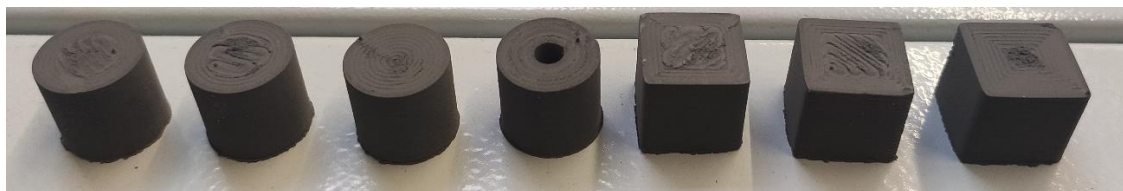
Figure 18: Tests of printing

ESTIA Addimadour is simply equipped with a cubic furnace given by Lynxter for the first trials. This oven is composed by porous walls with the possibility to have inert atmosphere and high temperature. The equipment used is visible on the **¡Error! No se encuentra el origen de la referencia.**.

Figure 19: Oven for the first trials

The filament supplier has provided debinding and sintering curves for each material. For H13 steel, 91 hours are needed to debind and sinter the part, see **¡Error! No se encuentra el origen de la referencia.**.
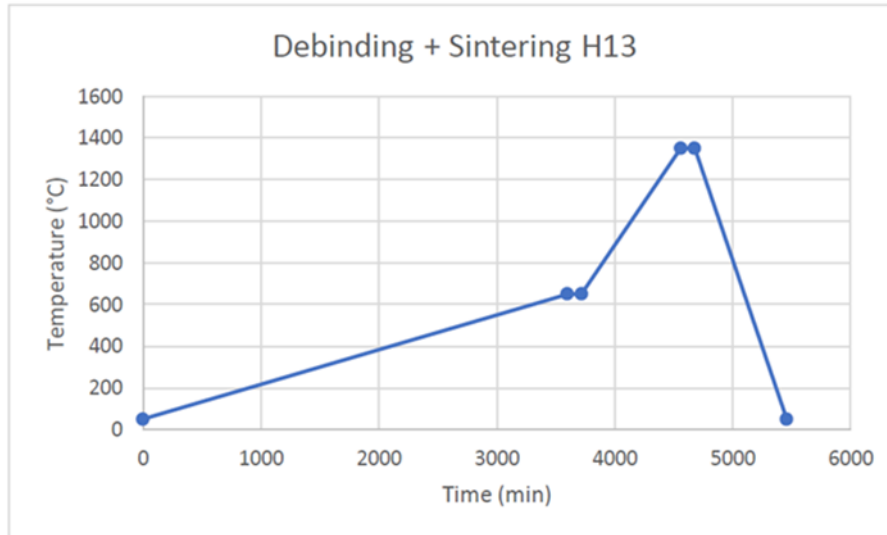
Figure 20: Example of H13 debinding/sintering curve

Despite numerous tests, the oven used does not provide satisfactory results, there remains: see **¡Error! No se encuentra el origen de la referencia.**.

- Cracks,
- Bubbles,
- Deformations,
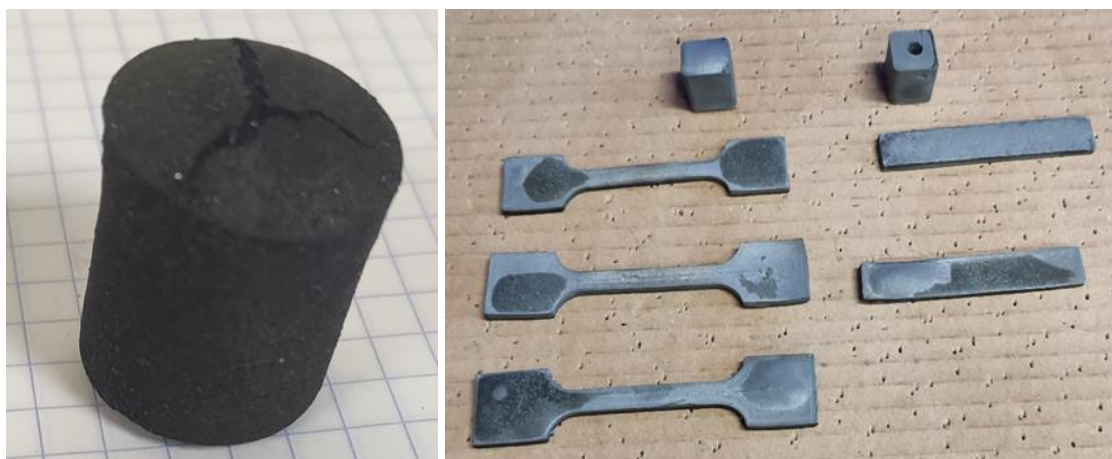- Polymer residues / carbonization,
- etc.

Figure 21: Example of debinding/sintering problems

To conclude with this equipment, the cycle to debind and sinter a part about 91h is too long and must be reduced to remain competitive. Indeed, this kind of cycle implies having a very high consumption of electricity and a very high consumption of gas: At

1.6L/min, it's about 8800L for one complete cycle which corresponds to approximately 1 gas cylinder of 50L at 200Bars.

Moreover, the part has very poor mechanical properties to use it as it is. A cubic oven with porous walls inside is not recommended for this application. The debinding is a key operation in the process. The quality of this operation is fundamental so as not to cause physical (cracking) or chemical (carburizing) damage to the part. A very large part of the defects which appear after sintering are generated by inadequate debinding.

3) Printing of samples to improve debinding and sintering

To improve the quality of the debinding and the sintering phase and to cover all the value chain of this new technology, a lot of samples have been printed with the Lynxter S600D and characterized in the facilities of CEIT, see **¡Error! No se encuentra el origen de la referencia.**.

Figure 22: Samples for improving debinding and sintering

3.1) *Optimization of debinding process*

In order to choose the correct debinding cycle thermogravimetric (TGA) test were carried out, figure 26. This test shows the binder mass loss due to applying a heat cycle (5 °C/min heating rate until 1000 °C in H_2 atmosphere). The first curve (orange) was carried out on an as-printed sample and showed two areas of greater mass loss approximately around (275 °C and 375 °C). The total mass loss in this samples was 9.2 wt.% and this was completely achieved around 500 °C.
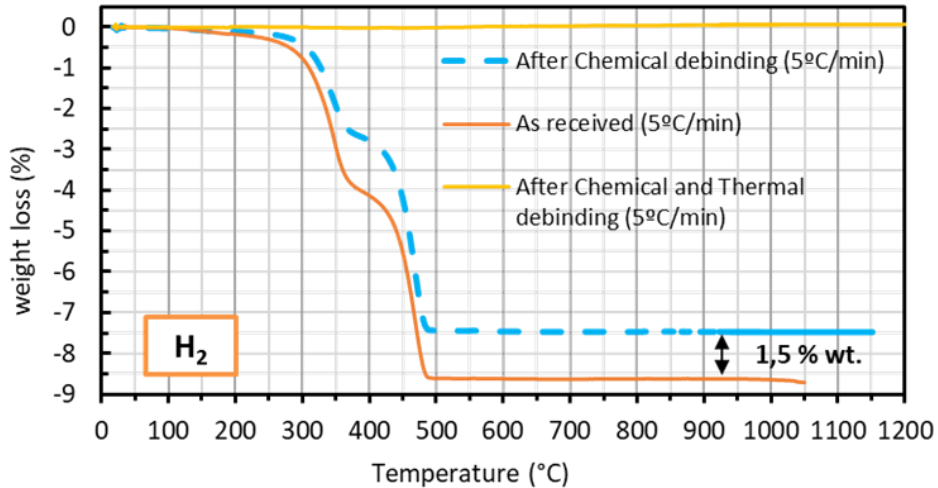
Figure 26: Thermogravimetry results of H13 samples. Orange: TGA cycle on as-received sample; Blue: TGA cycle after chemical debinding; yellow: TGA cycle in a sample after thermal debinding in a furnace.

Taking into account the TGA results, a debinding cycle with two holding steps (at 275 and at 375 °C) and maximum temperature of 550 °C, to ensure complete binder removal, was designed. In the first approach the heating rate used was 1 °C/min. This heating rate was proven to be too fast since samples showed presence of cracks and deformation, Figure 27. Thus, the cycle was optimised by reducing the heating temperature to 0.5 °C/min, Figure 28.

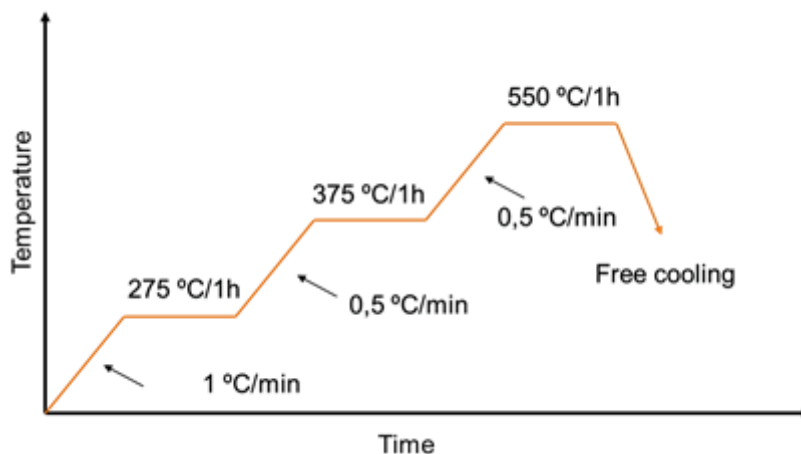*Figure 27: H13 samples after debinding with heating rate of 1 °C/min.*

Figure 28: Debinding cycle designed with TGA results for H13 samples.

Although cracks disappeared after the new thermal debinding cycle, samples still showed some deformations and bubbles (Figure 29a), and a new approach was used by introducing a chemical debinding before the thermal one.
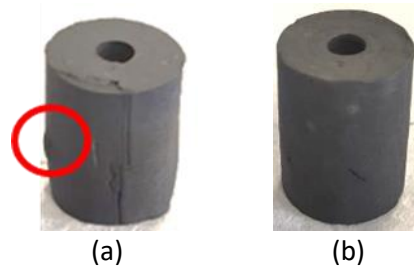

(a)   (b)

Figure 29: H13 samples after thermal debinding (a) and after chemical debinding + thermal debinding (b).

For **chemical debinding,** samples were immersed completely in isopropanol (Ethyl alcohol) for 5 h at 55 °C, see the laboratory set up in the following Figure 30. TGA analysed performed on samples with chemical debinding showed the same behaviour than as-received samples, with two different slopes, but with less amount (1.5 wt. %) of binder loss, Figure 26 blue curve. Although the mass loss different was very little, this step allows to remove the binder easier during the subsequent thermal debinding and thus the samples geometry reminds more stable and without bubble presence, Figure 29b.

Figure 30: Laboratory set up for chemical debinding.

Finally, thanks to applying the chemical debinding the subsequent **optimised thermal debinding** was able to be simplified by removing the two holding steps as showed in Figure 31. Thermal debinding at Ceit were carried out in a Limberg type furnace with

coupled metallic tube with inlet and outlet pipes for gas circulation. The cycles were performed in Arcal atmosphere (97,5 % Ar and 2.5 % H_2). After this cycle samples were again introduced in TGA cycles (yellow line in Figure 26) confirming the total binder removal during this optimised and simplified thermal debinding cycle.
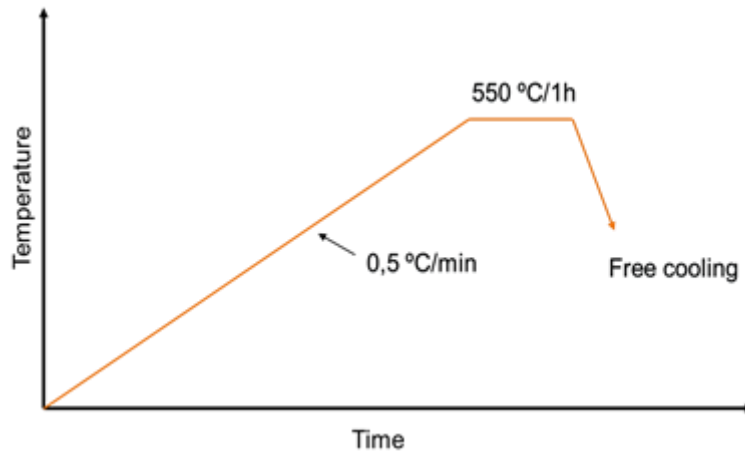

Figure 31: Simplified thermal debinding to be used after chemical debinding.

3.2) *Optimization of sintering process*

The sintering of H13 samples after chemical + thermal debinding were carried out in an MRF type furnace. Two sintering treatments (1350 °C and 1400 °C) were applied with same conditions, maintenance time of 2h and Arcal atmosphere (97,5 % Ar y 2.5 % H_2). The difference obtained with these two sintering cycles are explained in deliverable "2.1. Report of material for MAM".
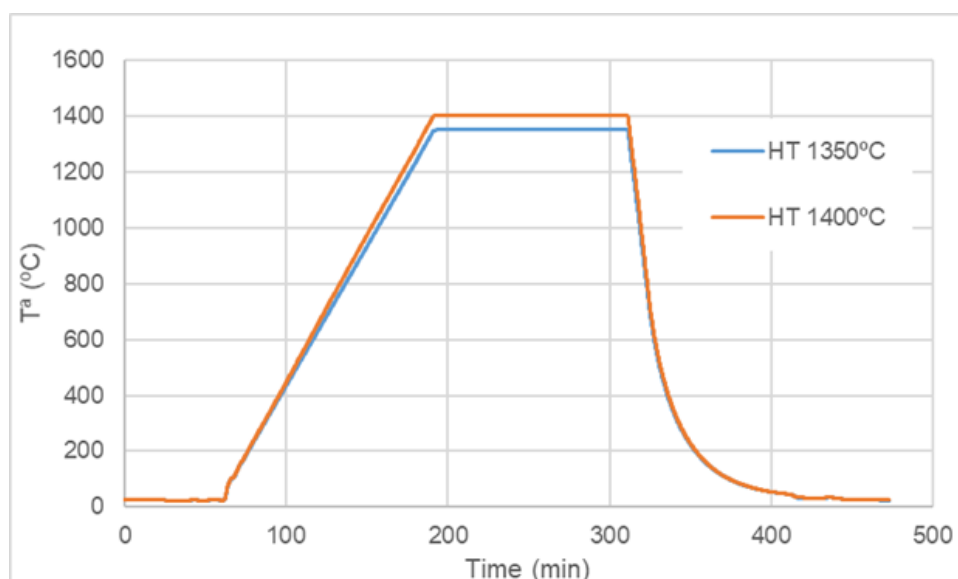
Figure 32: Sintering cycles (1350 °C and 1400 °C) applied to H13 samples after chemical + thermal debinding.

3.3) *HIP cycles*

In addition, to obtain a greater densification and to be able to close the internal porosity of the material, Hot Isostatic Press (HIP) cycle was performed at 1150 °C and 150 MPa (pressure applied with argon) with a 2h maintenance. 10 °C/min heating rate and free cooling was used for HIP cycle, Figure 33.
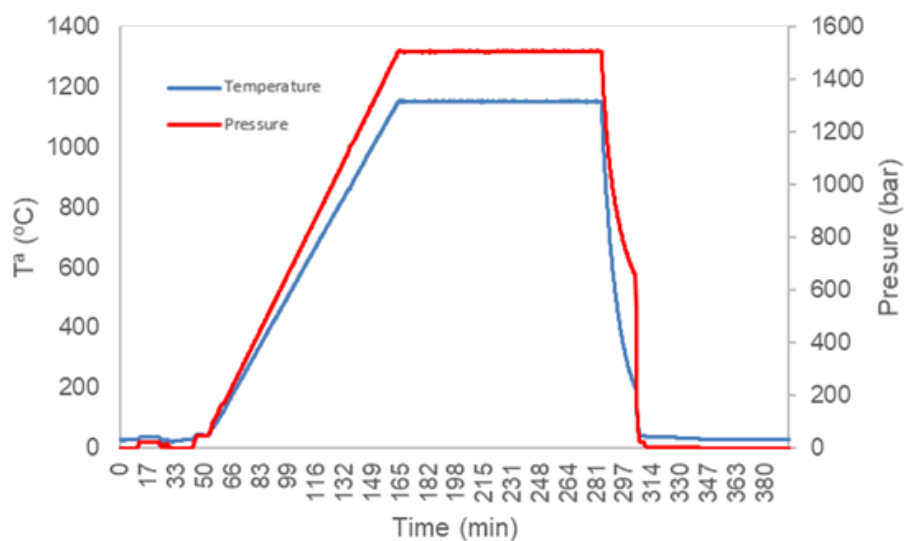

Figure 33: HIP cycle, 1150 °C, 2 h, 150 MPa, 10 °C/min heating rate and free cooling.

3.4) *validation of components*

The validation of the components was done, and the results are shown in Deliverable 2.1.

4) Redesign of the part

The proposed use case from SOMOCAP company had a conventional cooling channel inside the part, see **¡Error! No se encuentra el origen de la referencia.**. However, this simply straight hole for cooling is not enough and the cooling is not efficient: during the cooling phase, the polymer part reveals an ovalization and is not quite circular. The use of additive manufacturing technologies gives the option to perform conformal cooling. Hence a redesign of the internal cooling was done as shown in **¡Error! No se encuentra el origen de la referencia.**.
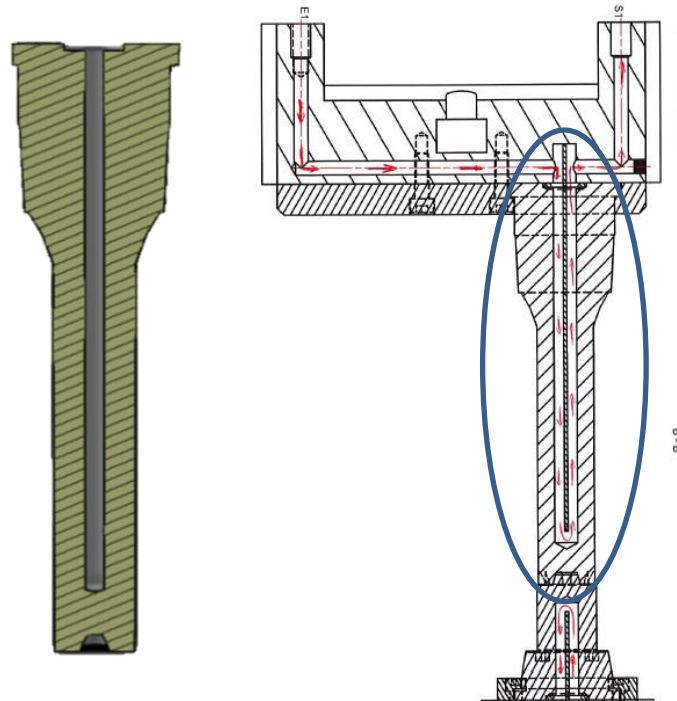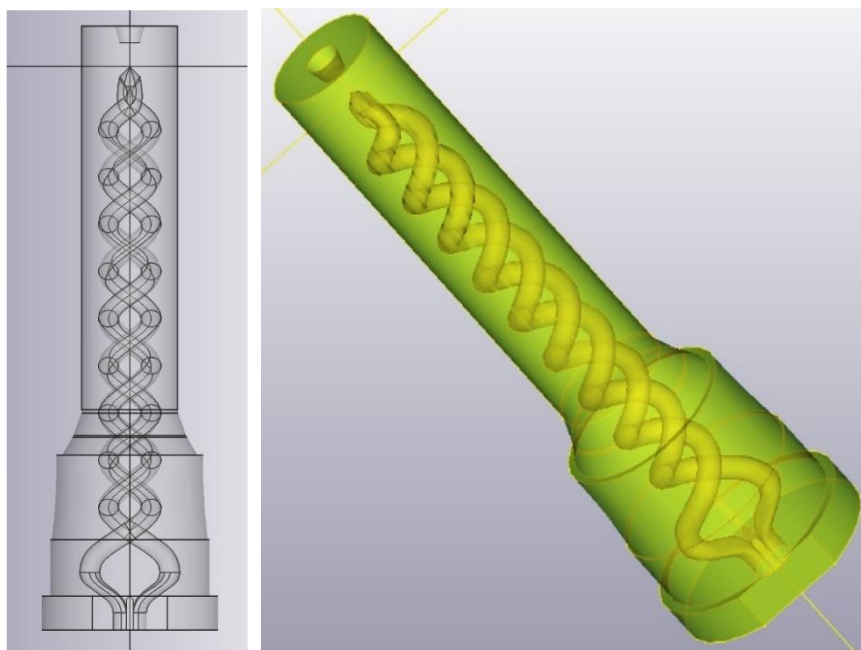
Figure 23: Original regulation

Figure 24: Conformal cooling

Also, and as with all MAM technologies, an extra thickness has been added for the machining step of the external, functional surface.

In this case, 2 mm has been added (see **¡Error! No se encuentra el origen de la referencia.**) to:

- Make sure there is enough material to be machined and no missing material.
- Anticipate possible deformations after debinding and sintering.
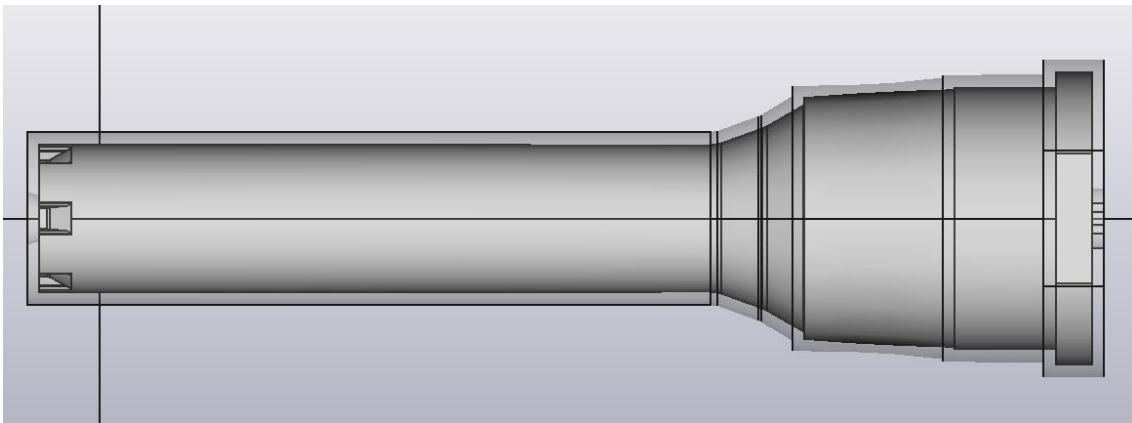

Figure 25: Overthicknesses for machining

For the parts manufactured by FFF process with Markforged Metal X equipment, the following method was applied:

➢ Manufacturing of samples manufacturing for both materials: 17.4-PH and H13.

Tensile samples manufactured in horizontal orientation, dilatometry samples, HIP samples with cylindrical shape and a centre hole and samples for microstructural study are shown in the Figure.

Figure 26. Tensile samples built in horizontal orientation.

  ➢ Selection of parameters

Table 3. Parameters selected for the manufacturing of samples.

Layer heigth (mm)	0,125
Filling method	Solid
Edge thickness (mm)	0,5-2
Roof and bottom thickness (mm)	0-2

  ➢ Redesign

The part had to be manufactured in horizontal orientation due to height restriction of the manufacturing chamber. Hence, cooling channels needed to be adapted to avoid supports inside. The adaptation consisted of choosing a drop shape, which means an auto supportable shape.

➢ Manufacturing of details to check the integrity of the channels and the absence of supports inside them was done.
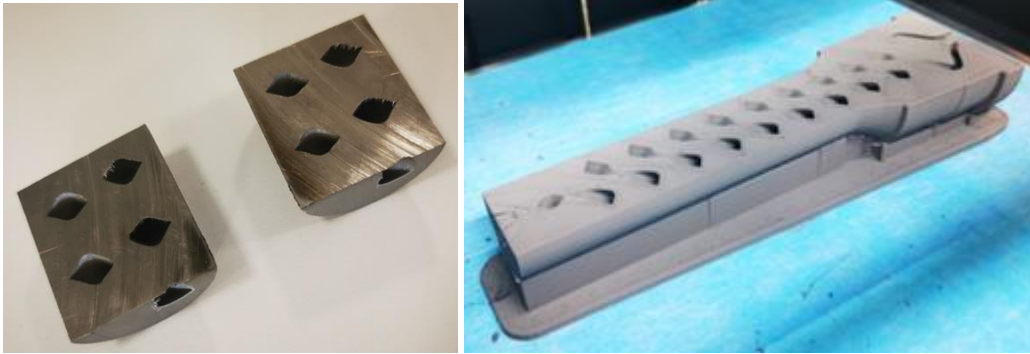

Figure 27. Details of the adapted cooling channels.

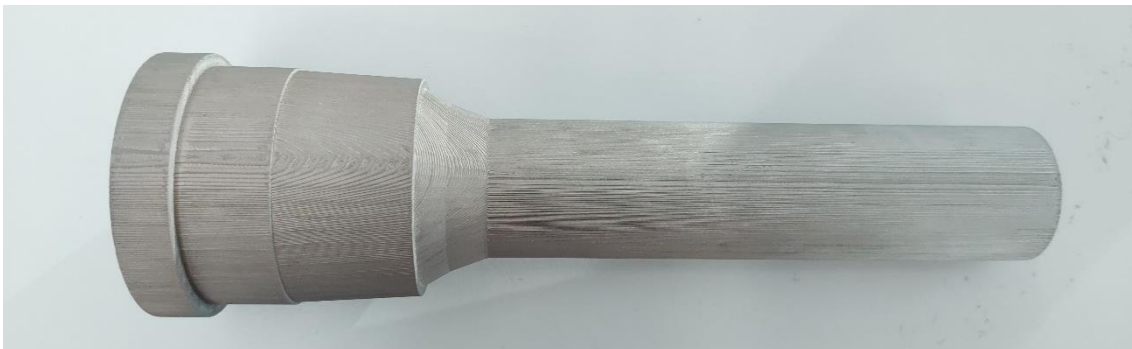➢ Manufacturing of demonstrators in both materials.

Figure 28. Manufactured part.

➢ Machining to remove the 2 mm of overthickness in the external surface and obtain a smooth surface.

The learnt lessons in the development of this demonstrative pilot are:

-Regarding Markforged machine, it is very closed, so the process cannot be improved. Due to dimensional restrictions in manufacturing chamber and oven, it had to be printed horizontally and hence an additional redesign in the channels had been applied to avoid supports.

-HIP helped closing most of the pores achieving around 98 % of density. Due to this, the mechanical properties were enhanced in a great amount.

Pilot PT2-VIDRIMOLDE

Manufacturing

Manufacturing of main body by L-PBF

The mold of Pilot PT2 was manufactured in two stages. First, the main body was manufactured by L-PBF in a XXX machine, at a local company (DRT), due to the part size. This body was manufactured using EOS StainlessSteel CX powder, a "tooling grade steel characterized having a good corrosion resistance, combined with high strength and hardness."[1]. Next, that body was added layers of Inconel 718 by Laser Directed Energy Deposition (L-DED).

Before the manufacturing of the part itself, the powder was analysed and L-PBF specimens were produced, to perform L-DED deposition tests. The results from the first task can be consulted in the deliverable D 2.1. REPORT ON MATERIAL FOR MAM. As for the deposition tests, they are described next.

L-DED deposition tests

The deposition tests were performed in a Trumpf TruLaser Cell 3000, with the base process parameters shown in Table XEF.

Table 1: L-DED process parameters.

Parameter	Value
Speed (m/min)	0.4
Spot diameter (μm)	2000
Laser output operating mode	Ring
Laser power (W)	800
Surface power density (W/mm2)	255
Mass stream (g/min)	5
Carrier gas flow (l/min)	4 (He)
Nozzle gas flow (l/min)	15 (Ar)

The following investigation will characterize the hybridization of L-DED with the L-PBF process. The objectives of this work are to clear the following process parameters:

- Thickness of the solid layer covering the inner lattice structure. The research will seek to reduce this thickness value while still preventing the creation of defects on the structure inside.

- Fabrication parameters for the L-DED process, being these the laser power (P), feed rate (F) and powder flow (Q).

Methodology: single clad tests

Single bead tests, combining the parameter sets described in Table XX with substrates of different thickness: 6, 1 and 0.7 mm were performed – Table YY. The fabricated beads have a length of 25 mm and have been centered on the surface area of 15mm x32mm.

	P (W)	F (mm/min)	Q (g/min)	P/F
Ref.	600	525	5.5	1.143
Reduced	500	525	5.5	0.952

Table 2: Reference L-DED process parameter set.

[1] EOS, EOS StainlessSteel CX Material data sheet.

N.	Test type	Parameter set	Substrate thickness (mm)
1	Single bead	Ref.	6
2	"	Reduced	6
3	"	Ref.	1
4	"	Reduced	1
5	"	Reduced	0.7

Table 2: Single bead testing plan parameters.

Methodology: overlapping tests

Layer tests using the reduced parameter values, on substrates of 2 and 1 mm of thickness were produced – Table XXX. These layers consist of 5 overlaid beads, with a distance of 1 mm between them. In order to simulate the effect a bigger deposition area would have on the fabrication process; a cooling time of 5 seconds is placed after each bead is deposited.

N.	Test type	Parameter set	Substrate thickness (mm)
6	Layer	Reduced	2
7	"	Reduced	1

Table 3: Layer testing plan parameters.

Methodology: single bead wall

Fabrication of a single bead wall using the reduced parameter values on a 2 millimeter substrate was performed – Table FFF. The wall consists of 20 layers of beads, deposited on the same direction and with a cooling time of 10 seconds between each of them.

N.	Test type	Parameter set	Substrate thickness (mm)
8	Wall	Reduced	2

Table 4: Layer testing plan parameters.

After the above test an analysis of the fabricated samples by metallographic analysis and the measurement of deformation caused by the residual stress of the process was conducted.

Results of deposition tests: *Single bead tests*

Figure XX depicts the metallographic analysis of the interface between the L-PBF substrate and the L-DED bead.
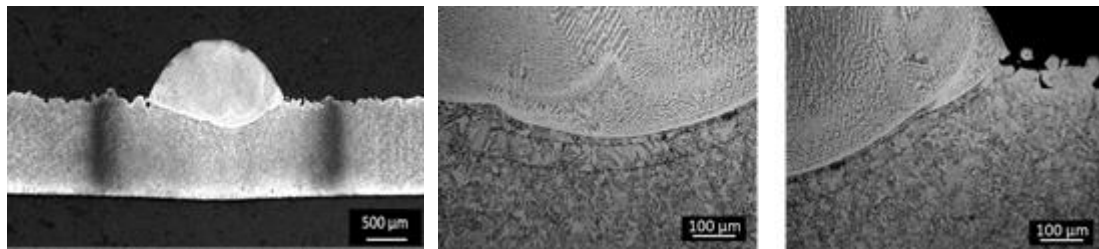

Figure 2: The L-PBF / L-DED interface.

From the observation of Figure XXX (right), it is possible to note two lines that distinguish a discontinuity in the substrate, following the dilution line. This could indicate the formation of micro-cracking on the substrate.

Table GGG shows the Heat-Affected Zone (HAZ) measurements. It is possible to observe that, for the thinner substrate, the HAZ is wider.

N.	Substrate thickness (mm)	HAZ Measurements (mm)
4	1	2.89
5	0.7	3.88

Table 5: Heat-Affected Zone (HAZ) measurements for tests 4 and 5.

Results of deposition tests: *Layer tests*

Figure XXX shows the cross section from the layer deposited on 2mm (up) and 1 mm (down) thickness base specimens. It can be observed that optimal process parameters for the L-DED process on a PBF substrate are the reduced ones from Table YY.
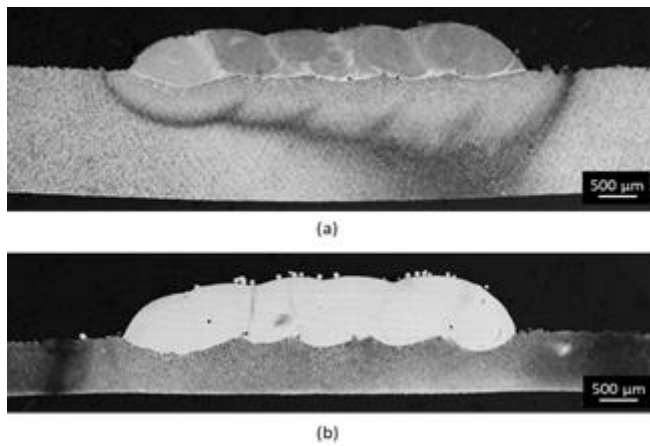

Figure 3: Cross-sections of the fabricated layers: (a) n. 6, and (b) n. 7.

Figure DXS shows samples 6 and 7 after deposition. A significant deformation is observed in sample 7. This is further illustrated in Figure FRD. In conclusion, fabrication on a substrate as thin as 1 mm is feasible but with a significant deformation on the part.

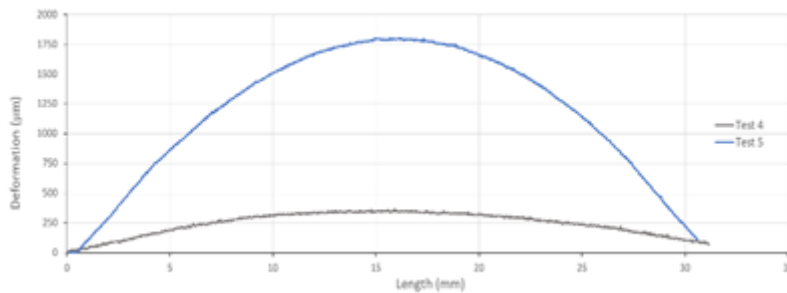*Figure 4: Samples 6 and 7 after deposition. The warpage observed is significant, especially on sample 7.*

Figure 5: Measurement of vertical deformation on samples 6 and 7 - Test 4 and 5, respectively.

Results of deposition tests: *Wall test*

The cross-section of the fabricated single bead wall is shown in Figure FRDS. Due to the fact that the thickness of the substrate used is larger than that of previous tests (2 millimeters), the HAZ is significantly reduced in comparison to them.
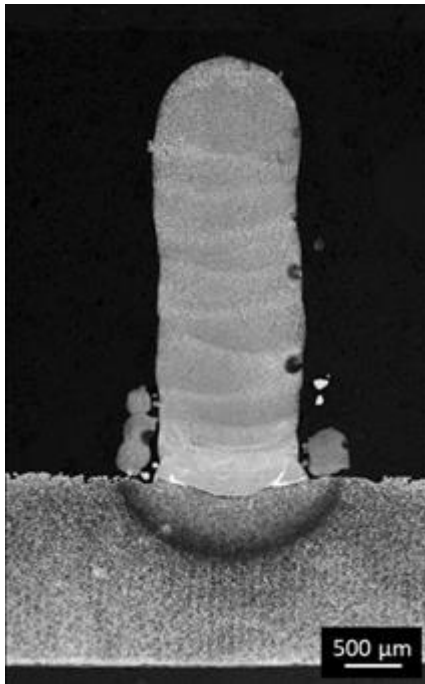

Figure 6: Wall test (test 8).

Results of deposition tests: *Temperature during fabrication*

Figure DKFN represents the temperature analysis during fabrication for samples 4 and 5, as an example. A higher temperature is verified on slimmer substrates.
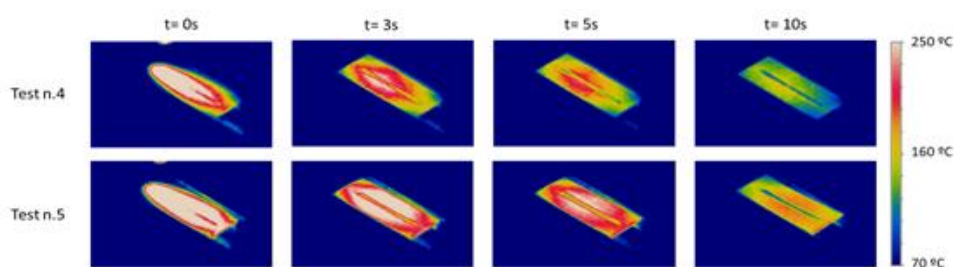

Figure 7: Temperature analysis during fabrication for samples 4 and 5

Figure RTGF represents the melt-pool temperature profile on the fabrication of n.4, as an example. It is observable that the temperature of the melt pool remains in-between the values of 2000-2300 °C in all cases.
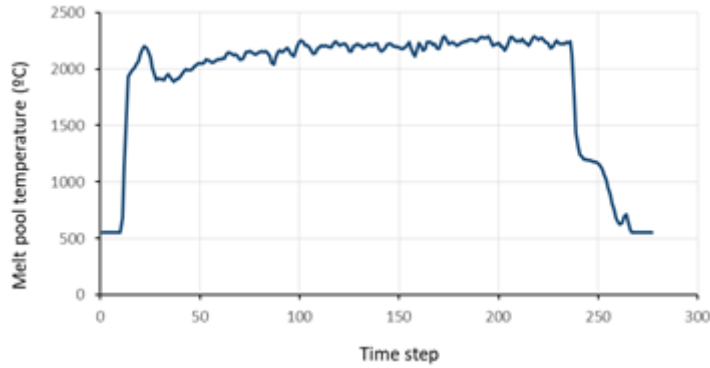
Figure 8: Melt-pool temperature profile on the fabrication of n.4.

Results of deposition tests: *Conclusions*

A Laser power (P) of 500 W, Feed rate (F) of 525 mm/min and Powder flow (Q) of 5.5 g/min are the optimal parameters for the deposition of material on thin substrates.

With these parameters, substrates as thin as 0.7 millimeters of thickness can be used in the fabrication of single beads.

In the case of layer fabrication the use of substrates of a thickness of 1 mm is possible, although the deformation of the substrate under those conditions must be taken into consideration.

Manufacturing results

Figure DCF depicts the mold after manufacturing by L-PBF. The part was then sent to UPV for L-DED deposition.

Figure 9: Mold for glass manufactured by L-PBF.

Figure FTR depicts the mold after depositon by L-DED.

Figure 10: Mold half after deposition by L-DED.

Post-processing.

The post processing of the L-PBF part involved the separation from the base plate, via wire EDM. This was performed at the same company (DRT) who possesses the appropriate equipment for this task. No heat treatment was performed.

The learnt lessons in the development of this demonstrative pilot are:

- The glass moulding technology has specific challenges that cause the alternative manufacturing of moulds by AM to be, in principle less atractive. These factors are the low price of the conventional mould and reduced cycle time (typically 5s) that leave less potential for improvement.
- The manufacture of a mould for glass using AM is time-consuming and has a very high initial cost. But the combination of the L-PBF and L-DED processes allowed to obtain a mould with better thermal performance (due to the conformal cooling channels) and probably with better life, as the full mould surface is now coated with a nickel-based alloy (whereas in the case of conventional moulds the coating is only at the mould surface edges)
- It is necessary to demonstrate, via pilot testing facilities, the performance and viability of this solution, particularly to glass parts manufacturers. Hopefully their hesitancy to allow in situ testing should be mitigated.

Interreg
Sudoe

ΛDDiTOOL

European Regional Development Fund

EUROPEAN UNION

www.additool.eu